Self-assembled guanosine-hydrogels for drug-delivery application: Structural and mechanical characterization, methylene blue loading and controlled release

Self-assembled Guanosine-hydrogels for Drug-delivery Application: Structural and Mechanical Characterization, Methylene Blue Loading and Controlled Release

Juliana S. Yoneda[1†], Daniele R. de Araujo[2], Fiorenza Sella[3], Gabriel R. Liguori[4], Tácia T. A. Liguori[4], Luiz Felipe P. Moreira[4], Francesco Spinozzi[3], Paolo Mariani[3], Rosangela Itri*[1]*

[1]Instituto de Fisica, Universidade de São Paulo, São Paulo, SP, Brazil;

[2]Universidade Federal do ABC, Santo André – Brazil;

[3]Dipartimento di Scienze della Vita e dell'Ambiente, Università Politecnica delle Marche, Ancona – Italy;

[4]Instituto do Coração (InCor), Hospital das Clinicas HCFMUSP, Faculdade de Medicina, Universidade de São Paulo, São Paulo, SP, BR.

* email corresponding authors: julianasakamoto@hotmail.com; itri@if.usp.br

†Present Address - Juliana Sakamoto Yoneda - Brazilian Synchrotron Light Laboratory (LNLS). Brazilian Center for Research in Energy and Materials (CNPEM), P.O. Box 6192, Campinas CEP 13083-970, SP, Brazil

Keywords: hydrogel, guanosine, G-quadruplex, drug delivery, pH-responsive

Abstract

The ability of guanosine derivatives (G) to form long, flexible, and interacting aggregates (the so-called G-quadruplexes) in water by self-assembly can be exploited to obtain multi-responsive hydrogels. Here, we investigate the potential application of Gua:GMP hydrogels as novel drug delivery systems. To this end, hydrogels prepared with distinct Gua:GMP molar ratios (1:1, 1:2 and 1:6) produced nanofibers disposed in swollen matrixes with different mesh-sizes as revealed by small angle X-Ray scattering (SAXS) and atomic force microscopy. The dye and photosensitizer Methylene blue (MB) and the pro-apoptotic protein cytochrome C (CytC) were used as cargo molecules. Interestingly, we show that Gua:GMP molar ratio leads to specific drug release mechanisms by rheology measurements, while the gel strength is tuned by electrostatic repulsion and van der Waals attraction between G-quadruplexes fibers. Noteworthy, the gel cohesion and the drug release are pH responsive. Furthermore, swelling, self-healing and cell viability features were also here investigated, qualifying the Gua: GMP hydrogel as an excellent biomaterial that can entrap and deliver key biomolecules in a sustained and responsive release manner.

1. Introduction

Hydrogels are enthralling biomaterials due to their characteristics such as biocompatibility, biodegradability, hydrophilicity, and non-toxicity. Several applications in medical and pharmaceutical fields have been indicated: indeed, the water-swollen structures can mimic native extracellular matrix or microenvironments of tissues, which make hydrogels excellent candidates for tissue engineering, 3D cell culture, and biosensors, as well as for controlled drug delivery purposes [1–5]. Self-assembled low-molecular-weight gelators are very interesting precursors for supramolecular hydrogels, bringing up an alternative to traditional polymeric hydrogels [6–8]. Indeed, hydrogels from the spontaneous self-assembly of low-molecular-weight gelators form via non-covalent forces as hydrogen bonds, π-stacking and van der Waals [9–13] and can be then considered smart materials owing to their unique properties as self-healing and external stimuli-responsiveness [14,15]. These properties encourage their applications as controlled and sustained drug release, for instance, in response to temperature or environment pH changes [16,17].

Self-assembling supramolecular hydrogels, stable at physiological pH and temperature and able to entrap up to 98% w/w of water, have been recently obtained by guanine and related nucleobases (Gs), both natural and chemically modified [18–21]. The hydrogel is formed because the guanine ability to self-assemble in aqueous solution via a unique topological diversity: *(a)* formation of cyclic planar units (G-quartets) through hydrogen-bonds according to the Hoogsteen scheme; *(b)* successive formation of long columns (G-quadruplexes) in the presence of appropriate counter-ions (as NH_4^+, Na^+ or K^+), stabilized by π-π stacking among the G-quartets piled one on the top of the others; *(c)* final formation of entangled supramolecular architectures stabilized by lateral column to column interactions [21–28].

Many strategies have been developed to fine-tune the chemical and mechanical properties of G-based hydrogels to make them usable under different experimental conditions [20]. For instance, isoguanosine [29] and guanosine-borate have been used to produce hydrogels with long time-stability [23,30]. Stabilization of guanosine monophosphate hydrogels by lanthanide ions [31] and by polyamine [32] has also been reported. Besides, the addition of silver ions to 2'-deoxy-2'-fluoroguanosine produced stable supramolecular hydrogel [33]. In the current case, hydrogels obtained by mixing in water guanosine 5'-monophosphate dipotassium salt (GMP) and guanosine (Gua) are considered. Indeed, such a system shows several advantages since it is composed of commercially available building blocks [18,34,35], and its thermo-associative and thermo-dissociative behaviors are strongly related to composition (see the phase diagram in ref. [18]). It should also be noticed that the hydrogel formation occurs by merely mixing the two precursor solutions: water-insoluble Gua dissolves in the mixture replacing GMP in the G-quartets, and gelation is induced because an uncharged molecule replaces a negatively-charged one. The reduction of electrostatic repulsive forces between G-quadruplexes and the appearance of attractive Van der Waals interactions favor G-quadruplex entanglement and hence the formation of a stable 3D network even at a water volume fraction as high as 0.99 [18].

Despite of this facile strategy without need of precursor chemical modifications to produce stable guanosine-based hydrogels, these have not been explored yet for biomedical and pharmaceutical applications. Henceforth, in this work, we provide evidence that binary Gua/GMP hydrogels can be promising candidates for drug delivery system. Three formulations were considered, e.g., hydrogels prepared at the Gua:GMP molar ratios 1:6, 1:2, and 1:1 (hydrogel 1:6 has the highest proportion of GMP, therefore the highest negative charge along the G-quadruplexes, while the 1:1 sample

presents the highest attractive potential [18]). Because charge modifications can modulate the G-quadruplex entanglement [18,36], these hydrogels are expected to be pH-responsive, highlighting their promising biomedical applications.

In the current work, we investigate the load and release of methylene blue (MB). It is an organic dye with an aromatic and positively charged structure, largely employed as photosensitizer (PS) too. The molecular weight of MB is 319.85 g mol^{-1} and it belongs to the phenothiazine family, being known as a DNA ligand [37,38]. MB can weakly bind to single-strand DNA due to electrostatic interaction or be intercalated into DNA double helix, preferably to G-C base pairs [39]. Also, MB interacts stronger with G-quadruplex compared to DNA double strand [40,41]. As a photosensitizer, it is FDA-approved drug [42–44] widely used in photodynamic therapy, with applications in clinic to treat cancerous and non-cancerous diseases [45–48]. In an interesting manner, the encapsulation of a PS into a hydrogel matrix may be a good strategy to increase the time retention of the PS in contact with the target tissue/cell due to the low fluidity of the hydrogel [49].

The protein cytochrome C (CytC) is also here investigated as a drug model for comparison purposes. CytC is a protein with 12kDa, positively charged at neutral pH and it can be found in the inner membrane space of mitochondria. It is involved in the oxidative phosphorylation and it is a crucial component of the intrinsic apoptosis pathway [50]. The intracellular delivery of CytC to cancer cells has been described to induce apoptosis for cancer therapy [50–53]. Therefore, novel biomaterials encapsulating and releasing key proteins can contribute to new strategies in cancer and other diseases treatment via cell death modulation.

2. Materials and Methods

2.1 Hydrogel preparation

Guanosines 5'-monophosphate (GMP), in the acid form (Santa Cruz Biotechnology, 98% purity), was converted into potassium salt by acid-base titration with 1M of KOH monitoring the pH until it reached 9.0. Then, it was precipitated by adding three volumes of absolute ethanol and collected by centrifugation in a microcentrifuge tube at a speed of 4000 rpm for 15 min. The pellet was washed two times with ethanol and lyophilized. The powder was re-suspended in distilled water at a concentration of 100 mg mL^{-1}. Guanosine (Gua) (Sigma, St. Louis, USA; 99% purity) was suspended in water at the concentration of 60 mg mL^{-1}. Hydrogels were prepared at three different Gua:GMP molar ratios (1:6, 1:2, and 1:1) by mixing into a glass vial the appropriate volume of Gua and GMP solutions and then adding distilled water to reach a final concentration of 50 mg mL^{-1}. As Gua is poorly soluble in water, errors in adding Gua to the mixture were minimized by pipetting the stock solution several times before delivery. Error on the Gua:GMP molar ratio not larger than 5% was estimated by gravimetric assay on delivery testing. Since samples prepared at high guanosine content appeared opalescent and macroscopically not homogeneous, the mixtures were heated up to 90 °C (i.e., till the formation of a fluid state) and then left to cool down at room temperature.

To prepare the samples in the presence of methylene blue (MB) or cytochrome-C (CytC), the final addition of distilled water was replaced by the addiction of MB or CytC solutions at the required concentrations. In any case, the Gua:GMP final concentration was 50 mg mL^{-1}.

2.2 Swelling and self-healing properties

The hydrogel samples were prepared and placed in a vial tube. Excess Milli-Q water or buffer at different pH values was mildly placed on the top of the hydrogel. At a constant time interval, the top solution was removed by turning the vial upside down. The remaining excess of water was dried with a paper towel, and the vial weighted. The solution was placed back on the top of the hydrogels, and the same procedure was followed over time. The swelling was expressed as a percentage of additional hydration.

To test the self-healing property, hydrogels prepared in the presence of CytC (red) and in the presence of MB (blue) were cut into small pieces, placed together, and let to stick. Pictures were taken over time to visualize the process.

2.3 Rheological measurements

Rheological analyses were carried out using an oscillatory rheometer (Kinexus La. Malvern Instruments) with a cone-plate geometry. Determination of the gel-sol phase transition temperature ($T_{gel\text{-}sol}$) was carried out by performing a temperature scan from 0 to 100 °C. Frequency sweep was also carried out with a range from 0.1 to 10 Hz at a fixed temperature of 37 °C. Parameters such as elastic modulus (G'), viscous modulus (G"), and viscosity (η) were determined using the rSpace for Kinexus® software.

2.4 Drug Penetration

To monitor the drug penetration, 80 μL of an MB solution (300 μM) or CytC solution (600 μM) were deposited on the top of hydrogel samples and allowed to penetrate the matrix. Photographs were taken over time to monitor the migration of the colored front. The values were expressed as a percentage of penetration.

2.5 Atomic Force Microscopy

AFM micrographs were performed at the Chemistry Department of FFCLRP-USP (BR) by using a Shimadzu SPM-9600 Scanning Probe Microscope (Shimadzu Corporation, Japan) operating in dynamic mode. Scanning was performed in air at 23 ºC by using silicon probes with a resonance frequency ranging from 324 to 369 kHz (Nanosensors, Switzerland). The scan rate was 0.2–0.5 Hz to prevent tip-induced sample deformations and/or damages. The values of the spring constants of the cantilevers were approximately 38 ± 8 N m^{-1}, and the values of their resonance frequencies were approximately 336 ± 67 kHz. The roughness values were determined by SPM Offline software, from Shimadzu. Hydrogel samples were diluted 100 times, dropped onto freshly cleaved mica substrates, and left to dry at room temperature before AFM imaging.

2.6 Small Angle X-Ray Scattering (SAXS)

SAXS measurements were performed on hydrogel prepared in the presence of MB using a NanoStar instrument (Bruker Corporation). The incident beam wavelength was λ = 1.54 Å, and the explored *Q*-range extended from 0.05 to 0.36 $Å^{-1}$ (*Q* is the modulus of the scattering vector, defined as $4\pi \sin\theta/\lambda$, where 2θ is the scattering angle). Scattering data were recorded on a 2-dimensional Bruker CCD camera of 2048 x 2048 pixels and corrected for background, detector efficiency, and sample transmission. The 2D data were then radially averaged to derive *I(Q) vs*. *Q* curves.

SAXS data analysis was carried out according to the Eq.(1)

$$I(Q) = \kappa n P(Q) S_M(Q) + B \qquad (1)$$

where *P(Q)* is the worm-like form factor considered to represent the G-quadruplexes, *n* is their number density, $S_M(Q)$ is the measured structure factor, κ is a calibration factor (necessary when data are not measured in absolute units), and B is the flat background

(due to possible uncertainty in buffer subtraction or transmission determination). In particular, the $P(Q)$ has been written as a product between the Pedersen-Schurtenberger infinitely thin chain form factor [54], $P_{PS}(Q)$, and the square of the local circular cross section, $A_{CS}(Q)$ (Eq.(3))

$$P(Q)=P_{PS}(Q)\left[A_{CS}(Q)\right]^2 \qquad (2)$$

$$A_{CS}(Q)=2\pi\int_0^{\infty}\left[\varrho(r)-\rho_0\right]J_0(Qr)r^2\,dr \qquad (3)$$

where $\varrho(r)$ is the radially symmetric electron density function in the direction perpendicular to the chain, ρ_0 is the bulk electron density and $J_0(x)$ is the zero-order Bessel function.

Here we approximate $\varrho(r)$ as

$$\varrho(r)=\sum_{g=1}^{N_g}\rho_g\varphi_g(r) \qquad (4)$$

where $\varphi_g(r)$ is the volume fraction distribution, in cylindrical symmetry, of the different chemical groups (*g)* that constitute Gua, GMP and MB, and ρ_g is the electron density of the *g*-group. The method is new and will be fully described in a forthcoming paper of some of us [Spinozzi and Mariani, in preparation]. Here, we only report that the volume fraction distribution $\varphi_g(r)$ is modeled as a peak formed by a combination of two error functions, $erf(r)$, and is normalized so that its integral over the whole volume of the G-quartet disk, of height *H* (corresponding to the stacking distance of 3.4 Å [55,56], returns the total volume occupied by all the n_g groups that are present in the G-quartet. Among the considered groups (the potassium cation, the guanine, the ribose, the phosphate, and the methylene blue), we also include the hydration water molecules, which fill the gaps in the sugar and phosphate domains and could possess a relative mass density, d_{HW}, slightly different from 1, as already demonstrated [57]. Fitting

parameters of the model are the average distance of each *g*-group from the axis center, r_g, the half-wideness and the smoothness of the peak, w_g and σ_g. From their values, it is possible to derive the hydrophobic radius R_h and the whole cylinder radius *R*. Fitting parameters related to the Pedersen-Schurtenberger model are the length b of the statistical segment (Khun length) and their number n_b, whose product defines the contour length $L = n_b b$ [54].

The measured structure factor is expressed by Eq. (5)

$$S_M(Q) = 1 + \beta(Q)[S(Q) - 1] \qquad (5)$$

where $\beta(Q)$ (Eq. (6) and Eq.(7)) is the coupling function that, according to [58], we have approximated by the one of a regular right cylinder of length *L* and radius *R*,

$$\beta(Q) = \frac{\left[\int_0^{\frac{\pi}{2}} f(Q,\beta)\sin\beta\, d\beta\right]^2}{\int_0^{\frac{\pi}{2}} [f(Q,\beta)]^2 \sin\beta\, d\beta} \qquad (6)$$

$$f(Q,\beta) = 2\pi R^2 L \frac{\sin\left(\frac{1}{2}QL\cos\beta\right)}{\frac{1}{2}QL\cos\beta} \frac{J_1(QR\sin\beta)}{QR\sin\beta} \qquad (7)$$

$J_1(x)$ being the first-order Bessel function. The particle-particle structure factor, $S(Q)$, refers to interactions among the entangled worm-like chains or the knots observed in the hydrogel [36], and then has been approximated by a fractal distribution of inhomogeneities (Eq. (8)), according to [59],

$$S(Q) = 1 + \frac{1}{(Qr_0)^D} \frac{D\Gamma(D-1)}{\left[1 + (Q\xi)^{-2}\right]^{\frac{D(D-1)}{2}}} \sin\left[(D-1)\tan^{-1}(Q\xi)\right] \qquad (8)$$

In this equation, D is the fractal dimension (comprised between 1 and 3), r_0 is the effective radius of the inhomogeneity, and ξ is the so-called correlation length, representing the average distance among the scattering inhomogeneities.

To note, the number density n of the particles is calculated on the basis of the molar concentrations of Gua and GMP (Eq.(9)),

$$n=(C_{Gua}+C_{GMP})/(4L/H) \qquad (9)$$

In a simple approach, the bounding of the MB molecules with the G-quartets can be rationalized on the basis of the simple equilibrium processes involving separately Gua (Eq. (10)) and GMP (Eq.(11)) such that

$$Gua+MB \leftrightarrows Gua-MB \; K_{Gua}=\exp\left(-\Delta G^0_{Gua}/RT\right)=\frac{C_{Gua-MB}}{C_{Gua,u}C_{MB,u}} \qquad (10)$$

$$GMP+MB \leftrightarrows GMP-MB \; K_{GMP}=\exp\left(-\Delta G^0_{GMP}/RT\right)=\frac{C_{GMP-MB}}{C_{GMP,u}C_{MB,u}} \qquad (11)$$

where $C_{Gua,u}$ and $C_{GMP,u}$ represent the concentrations of Gua and GMP unbound to MB and$C_{MB,u}$ is the free MB in solution. R is the universal gas constant and T the absolute temperature. In the limit of our experimental conditions, that is $C_{MB} \ll C_{Gua}$ and $C_{MB} \ll C_{GMP}$, we can easily derive the number of MB $(n¿¿MB)¿$ (Eq.(12)) per G-quartet,

$$n_{MB}=\frac{4C_{MB}}{C_{Gua}+C_{GMP}}\frac{C_{Gua}\exp\left(-\Delta G^0_{Gua}/RT\right)+C_{GMP}\exp\left(-\Delta G^0_{GMP}/RT\right)}{1+C_{Gua}\exp\left(-\Delta G^0_{Gua}/RT\right)+C_{GMP}\exp\left(-\Delta G^0_{GMP}/RT\right)} \qquad (12)$$

as a function of the two standard Gibbs free energy changes ΔG^0_{Gua} and ΔG^0_{GMP}.

All fitting parameters were obtained from the model fitting to the experimental data by means of GENFIT software [57].

2.7 In-vitro drug release

2.7.1 Membrane diffusion in vertical Franz-type cells

A membrane diffusion model in vertical Franz-type cells with 1.76 cm^2 (Microette Plus®, Hanson Research, CA, USA) and cellulose acetate membranes (MWCO 1000 Da) were used for i*n vitro* MB release assays. The hydrogel prepared in the presence of MB (0.5 g) was placed in the donor compartment, and the receptor was filled (7 mL) with water, kept at 37 °C under magnetic stirring (350 rpm). Aliquots of 1 mL were taken from the receptor compartment at different intervals of time up to 24 hours and analyzed by UV-Vis spectroscopy (Abs at λ = 665 nm). The MB concentration (c) was calculated using a calibration curve (¿|0.0154 c) with $R^2 = 0.997$. The measurements were performed in triplicate.

Release mechanisms were verified according to Zero-Order (Eq.(13)), Higuchi (Eq.(14)), and Korsmeyer-Peppas (Eq.(15)) models, as described respectively below.

$$Q_t = Q_0 + K_0^t \qquad (13)$$

where Q_t is the cumulative amount of drug released at time t in the Zero-Order model, Q_0 is the initial amount of drug, K_0 is the zero-order release constant, and *t* is the time.

$$Q_t = K_H t^{0.5} \qquad (14)$$

where Q_t is the amount of drug released in the Higuchi model and K_H is the corresponding release coefficient. In this case, the rate of release is linear as a function of the square root of time (t), and the drug is the only component that diffuses through the medium.

The mechanism of release is described as a diffusion process according to Fick law in the Korsmeyer-Peppas model as

$$\frac{M_t}{M_\infty} = K_{KP} t^n \qquad (15)$$

where $\frac{M_t}{M_\infty}$ is the fraction of drug released at time t, K_{KP} is a rate constant and n is the release exponent. Fickian diffusion is represented by a value of n < 0.45. If 0.45 < n < 0.89 an anomalous (non-Fickian) diffusion is the mechanism, while n = 0.89 represents the case-II transport, and n > 0.89 the super case-II transport.

2.7.2 In-vitro dissolution assays

A membraneless model was also used. In this system, the hydrogel sample was placed in a small glass container fixed on the bottom of a beaker. 10 mL of water or buffer (10 mM glycine-HCl pH 3.0, 10 mM sodium acetate pH 5.5, 10 mM sodium phosphate pH 7.4, and 10 mM sodium borate pH 9.0) were placed in the beaker on the top of the sample. This was kept under magnetic stirring at 37 °C. 1 mL of the surrounding solution was taken time on time, and the absorbance (670 nm for MB, or 412 nm for CytC) was recorded to acquire the amount of drug released. 1 mL of the buffer was replaced, and the dilutions were taken into account to do the calculation of the cumulative drug released at a determined time. The measurements were performed in triplicate.

2.8 Cell Viability Assessment

Adipose tissue-derived stromal cells (ASC), isolated from human subcutaneous fat acquired through liposuction, were used to assess cell viability in the presence of hydrogel. Note that the use of adipose tissue as a source of ASC was approved by the local Ethics Committee of the University of São Paulo Medical School (project number 4654/18/005), given that the material was considered as anonymous waste material. For all the anonymous donations, patients had provided written informed consent as part of their surgical admission procedure.

ASC were isolated as previously described [60–62]. For assessment of cell viability, ASC were seeded in 96-well plates with a seeding density of 1,000 cells/cm^2. After 24 hours, the culture medium was added with the hydrogel samples at increasing concentrations (0.1%, 1% e 10% v/v). Conventional DMEM culture medium and DMEM with 1 mg/mL of doxorubicin (Laboratório Bergamo, Taboão da Serra, Brazil) were used as the positive and negative control, respectively. After 48 hours of culture, cells were washed with PBS and analyzed using the LIVE/DEAD™ Viability/Cytotoxicity Kit for mammalian cells (L3224, ThermoFisher, Waltham, USA), according to the manufacturer's instructions. After incubation, cells were washed with PBS and immediately microphotographed in an inverted microscope Zeiss Axiovert 200 (Jena, Germany) equipped with a Zeiss AxioCam digital camera (Jena, Germany). A Ph2 10× objective was used either in phase contrast (illumination with a mercury lamp HBO 103 W) or in fluorescent mode with the filter set for excitation at 470/550 nm and emission at 525/605 nm, for the live/dead cells, respectively. The number of cells expressing the green and red staining was quantified, and the number of viable cells was expressed as the percentage of cells expressing the green, but not the red fluorescence.

2.9 Cell Culture on G-Quadruplex Hydrogels

For the evaluation of culture potential on top of the gels, wells of 96-well plates were covered with 100 μL of hydrogel samples. Previously, all the hydrogels were liquefied by heating to 80 ºC for 30 minutes and sterile-filtered with 0.22 μm polyethersulfone (PSE) filters. After pipetted into the wells, the liquefied hydrogels quickly turned into solid hydrogels. ASC were seeded at 3,000 cells/cm^2 seeding density. Cells were cultured in DMEM medium added of supplements, as described

above, at 37 ºC in a humidified incubator with 5% CO_2. After 48 hours under culture, cells were fixed with 4% paraformaldehyde in PBS for 30 minutes and stained with neutral red stain. Briefly, cells were washed with PBS, and the neutral red solution (1 mg/mL) was added to the wells and incubated for 2 hours at 37 ºC, then the staining solution as removed, and cells were washed with PBS. Microphotography images were acquired with an Olympus CKX53 inverted microscope.

3. Results and Discussion

The ability of guanosine and its derivatives to self-assembly into G-quadruplex structures is strongly related to the formation of supramolecular hydrogels. As previously shown, GMP in water presents a lyotropic liquid crystalline polymorphism determined by the formation of G-quartets and then G-quadruplexes [55,56]. On the contrary, Gua is poorly soluble in water. Our strategy was mixing both Gua and GMP to form G-quadruplexes, which spontaneously entangle into a 3D network. Indeed, GMP helps solubilization of Gua, which enters in the formation of the G-quartets; concomitantly, Gua helps hydrogel formation, since the substitution of GMP by a neutral molecule impairs the electrostatic repulsion and favors the appearance of cross-links and knots.

In the present work, we have chosen three hydrogels prepared at different Gua:GMP ratios (1:1, 1:2, and 1:6) at 95% water, to evaluate how their distinct features, like thermal stability, mesh-size, softness, impact on the encapsulation and release of drug models. Initially, we have characterized the hydrogels considering macroscopic properties such as swelling and self-healing. We studied the inner structure and the

rheological aspects, we assessed the cytotoxicity, and finally, we considered the drug loading and release capacities.

3.1 Swelling, erosion, and self-healing

The hydrogel swelling behavior (i.e. the ability of the gel to absorb water without breaking the 3D network) has been analyzed on the 1:1, 1:2, and 1:6 Gua:GMP samples. Results obtained using pure water are shown in **Figure 1a**. The hydrogel 1:6 did not show any water-absorbing capacity and erosion occurred in the first 8 hours of assay. On contrary, the Gua:GMP 1:1 and 1:2 samples swelled and showed similar behaviors over 100 hours, when the water concentration reaches a weight composition of more than 98%. This agrees with our expectation, since it was previously hypothesized that the Gua:GMP ratio modulates the interaction among the G-wires [18,36]. For higher GMP, therefore less Gua, (Gua:GMP = 1:6) the electrostatic repulsion is predominant, and the gel matrix cohesion is impaired which hampers the swelling capacity. By the other hand, diminishing GMP and increasing Gua, (Gua:GMP = 1:2, 1:1) the electrostatic repulsion is harmed and the hydrophobic interactions among Gua take place, increasing the gel cohesion and, therefore, the water absorbing capacity.

It is worth mentioning that the swelling may induce Gua phase-separation and precipitation on the 1:1 hydrogel since some white points were observed after 100 hours (Gua it-self is insoluble and needs GMP to be solubilized). This is reasonable because this sample has the lowest proportion of GMP, which could be insufficient to guarantee the presence of stables G-quartet. On the other hand, the 1:2 sample stays swollen (up to 99% w/w of water) and stable over several weeks, without precipitation.

As the GMP negative charges along G-quadruplexes are one of the main parameters controlling the hydrogel entanglement, the swelling observed using different

pH buffered solutions could be different. The swelling ability of the 1:2 and 1:1 samples was then measured using different buffers at pH of 3.0, 7.4, and 9.0. As shown in **Figure 1b**, the swelling behavior of the 1:1 sample using buffers at pH 3.0 and 7.4 was similar up to 120 hours (the hydrogel mass triplicated in both cases). After 140 hours, the hydrogel started to lose mass at pH 3.0, while the swelling proceeded at pH 7.4. At neutral pH, the hydrogel showed a four-fold mass increase in 10 days, reaching the limit of swelling (see also **Figure 1a**). It can be concluded that at acid pH, the equilibrium is shifted towards to protonation of GMP phosphate group, hampering the electrostatic repulsion among the G-nanofibers and hence, the tangle becomes tighter, limiting the water entrance.

Further, the sample 1:1 has an equal amount of Gua and GMP and, consequently, a slight charge unbalance may interfere in the hydrogel stability. The swelling capacity was higher at pH 7.4 since the entanglement degree is probably kept the same in this neutral environment. At pH 9.0, a very low swelling capacity was detected. The gel doubled in mass in the first 5 days, and then it started eroding. Likely, in alkaline conditions, there is an equilibrium shift towards deprotonation, increasing the negative charge along the G-quadruplexes. This favors repulsive interactions, and then an increase of the mean mesh distances: water entrapment probably triggers the matrix disruption. The sample 1:2 was submitted to the same procedure, and a similar behavior was observed (see **Figure 1c**). In acid pH, the 1:2 hydrogel intumesced up to 24 hours, and then it was disrupted. In alkaline conditions, the sample swells up to 6 hours, followed by erosion until it is completely destroyed. The swelling capacity for the 1:2 was higher at neutral pH, too, with a swelling up to twice the initial mass in 5 days and maintenance over weeks (**Figure 1c**). Photographs of the samples during the swelling experiment can be seen in **Figure S1** in the Supplementary Material (SM).

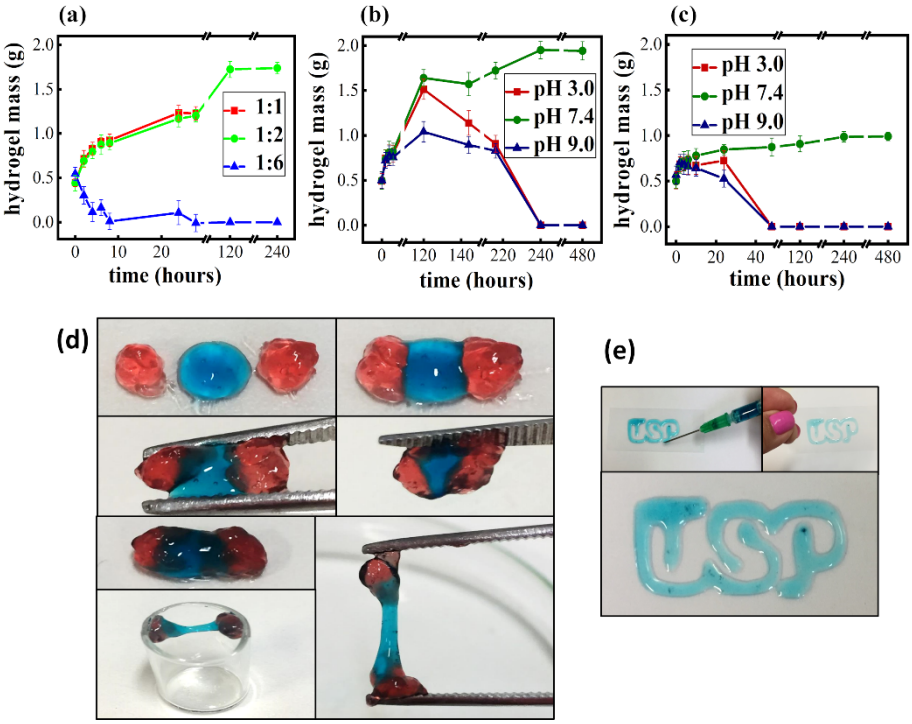

Figure 1. Swelling behavior and demonstration of the self-healing property of the Gua:GMP hydrogels. (a) Intumescence of the three gels: 1:1 - red; 1:2 - green and 1:6 - blue, in pure water (pH~6.0). Swelling behavior of the hydrogels (b) 1:1 and (c) 1:2 with buffer at three different pHs: 3.0 - red, 7.4 – green, and 9.0 – blue. The experiment was performed in triplicate. Averaged values are displayed, and the error bars considered the minimum and maximum measured values. (d) Optical images showing three pieces of hydrogel colored with methylene blue (blue) and cytochrome C (red) put in contact and then the healed piece. The restored hydrogel was taken with a tweezer, and the elasticity of the hydrogel was observed. (e) University of São Paulo – USP logo: hand drawing with the 1:1 gel, colored with methylene blue, through a syringe/21G needle.

Self-healing is the built-in ability of a material to spontaneously and automatically repairs physical damages. This phenomenon enhances the lifetime of that material and opens the possibility for many applications [3,63,64]. Self-healing is here shown on Gua:GMP 1:1 hydrogel, taking advantage of the red and blue colors obtained after preparation in the presence of CytC and MB, respectively. After equilibration, three pieces of hydrogels (one blue between two reds), were put in contact with each other, as

shown in **Figure 1d**. Because of the dynamic linkages of supramolecular non-covalent interactions, the three pieces stick together instantly upon they were joint. The self-healed piece was taken with a tweezer to show that the hydrogel maintained stuck; it should be noticed that even pulled with the tweezers, the hydrogel stretches and stays in this elongated form (**Figure 1d**).

Il should be observed that flexibility is however, associated with an intriguing fluidity so that the Gua:GMP (1:1) hydrogel can be used as an injectable material. **Figure 1e** shows that the hydrogel can be injected through a syringe with a 21G needle (the needle with the largest commonly used gauge for medical intramuscular injection). As with an ink, it is then possible to *write on a paper*. It should be remarked that the three investigated samples were all easily injected through a 21G needle, but 1:2 and 1:6 were too soft to be taken with a tweezer. Such findings are quite relevant since they imply that Gua:GMP hydrogel can be applied *in situ* as injectable formulations, without significant loss of mechanical properties [65–68] (see below).

3.2 Structural and mechanical properties

3.2.1 Structural insights of drug-loaded hydrogels: AFM and SAXS results

Firstly, the self-assembly of Gua/GMP was confirmed being due to the formation of G-quartets by X-Rays diffraction (XRD). A peak positioned at the angle around 2θ = 28°, which can be associated with the fingerprint of quartet stacking of 0.33 nm distance, was observed (Figure S2, SM). Then, the hydrogel structural properties were analyzed by AFM and SAXS. AFM images from MB-loaded hydrogels display long and flexible G-quadruplexes and the presence of knots (**Figure 2**), similarly as MB-free Gua:GMP hydrogels previously imaged [18]. Therefore, such results give us support to

infer that the MB incorporation into the hydrogel does not alter the guanosine ability to form stable quadruplexes organized in a 3D network.

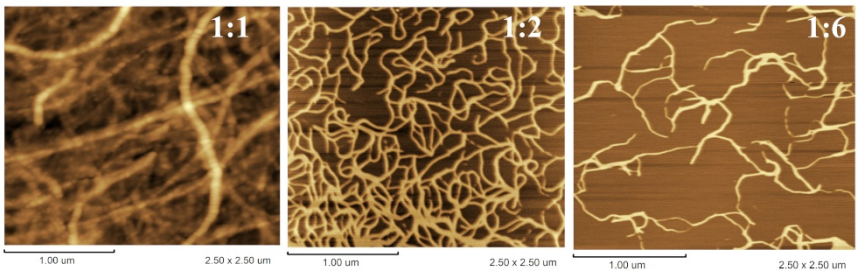

Figure 2. G-quadruplex fibrils detected by AFM. Hydrogels prepared at different Gua:GMP molar ratios: 1:1 (left), 1:2 (middle) and 1:6 (right) in the presence of 100 µM of MB. Similar patterns were observed in MB-free Gua:GMP hydrogels [18].

SAXS curves from MB-absent and MB-loaded Gua:GMP hydrogels are shown in **Figure 3.** As one can observe, the major differences among the SAXS data are due to changes in the Gua:GMP molar ratios, while variations with MB concentrations are not visible. As indicated in the *2.6 section*, data were analyzed according to the model described by Eqs. 2-4 and 8: worm-like particles interacting through a fractal model. To fit the data, a global fit strategy has been adopted, allowing to evaluate the optimum values of adjustable parameters that are in part considered to be the same for all samples or a sub-set of samples and in part assumed to change with both $x = C_{GMP}/C_{Gua}$ and C_{MB}. Common parameters for all the 12 SAXS curves were the scaling factor κ, the molecular volumes v_g of all the groups, which are optimized in a narrow range within literature data [69] and the two Gibb's free energy changes ΔG^0_{Gua} and ΔG^0_{GMP} (Eqs. 11-12), which describe the MB/Gua and MB/GMP interactions.

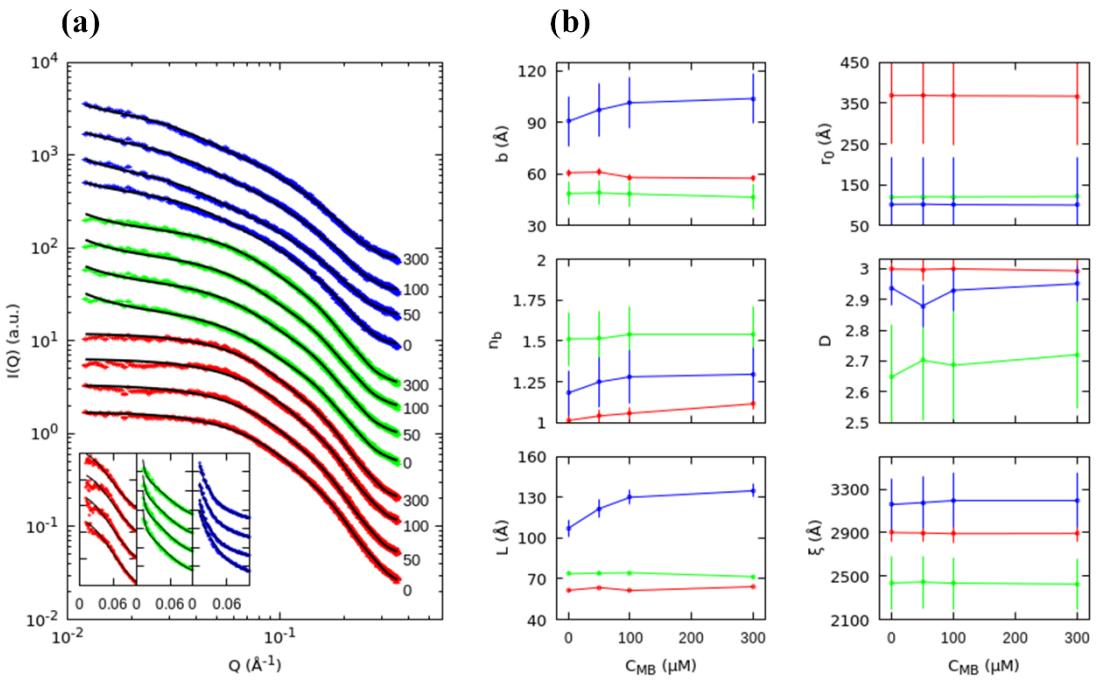

Figure 3. (a) SAXS curves, shown as log-log plots, for 1:1 (red points), 1:2 (green points) and 1:6 (blue points) MB-loaded Gua:GMP samples, neutral pH, at the different values of MB shown beside each curve in μM. Curves are multiplied by a factor 2 each on the top of the other for clarity. In the inset, data and best fits are reported in lin-lin plots, by adding a factor 0.5 among the curves for clarity. (b) The six panels on the right report the dependency on the MB concentration of the main fitting parameters: b (Khun length), n_b (number of segments), L (contour length), r_0 (effective radius of the inhomogeneity), D (fractal dimension) and ξ (correlation length).

Fitted model curves are superposed to SAXS data in **Figure 3**, and the goodness of the fit can be appreciated. Concerning fitting results, the main fitting parameters are reported as a function of MB concentration in the same figure, the common fitting parameters are reported in **Table 1,** and radial volume fraction distributions of the groups and the corresponding electron densities are shown in **Figure 4** and **Figure S3** in the SM, respectively. The main single fitting parameters show a very weak dependency on MB concentration, probably due to the very low amount of employed MB (300 μM, three orders of magnitude lower than the total concentration of Gua and GMP, 140 mM). However, a slight variation in the Khun length and in the number of statistical segments as a function of C_{MB} is observed in the case of the 1:6 hydrogel: the

final effect is a (small) increase of the quadruplex rigidity induced by MB, probably accentuated by the low stability of the Gua:GMP 1:6 hydrogel. Indeed, the 1:1 and 1:2 hydrogels show the shortest value of the segment length (b ≈ 50-60 Å) while the 1:6 sample a rather high value (around 100 Å): taken together, these results suggest that by increasing the GMP content, the worm like quadruplexes become more rigid.

Concerning the quadruplex-quadruplex interactions, as expressed by the structure factor parameters, fractal dimension (D) between 2.6 and 3.0 were found, confirming the substantial 3D nature of the hydrogel network. Gua:GMP 1:1 hydrogel shows the greatest values of the inhomogeneity radius r_0 (around 370 Å), while 1:2 and 1:6 hydrogels exhibit values close to 100 Å: this result is in full agreement with AFM observation, in which the 1:1 sample showed a very pronounced aggregation behavior, owing to the low net charge of the quadruplexes, which impairs repulsion and favors the hydrophobic interactions [18,36]. Regarding the correlation length ξ, results are similar for all the gels, being comprised between 2400 and ca. 3200 Å.

The volume-fraction distribution of the different chemical groups is plotted in **Figure 4** as a function of the radial distance from the quadruplex center. Each panel refers to samples with different values of the Gua:GMP ratio and the MB concentration. In detail, the derived volume-fraction profiles show the following properties: i) a very similar distribution is observed for the potassium (magenta curves), with a high and narrow peak centered in the center of the G-tetramer; ii) for the guanine (gold curves), a band centered at around a distance *r*=5 Å from the center of the G-tetramer, independent of hydrogel composition, is observed; iii) there is a complete absence of water in the region where the G-quartets are located (turquoise curve); iv) on the other side, the ribose distribution peak (red curves) changes in shape but not in position for the different samples, probably reflecting the different structural order around the G-quartet

region when the Gua:GMP ratio is changed; v) finally, the MB distribution curves (blue curves, which have been multiplied by a factor of 600 to amplify the signal) show that the MB position mainly overlaps with the ribose and phosphate groups, with some very slight differences related to the Gua:GMP ratio and MB concentration. It should be remarked that docking simulation showed that MB interacts with G-quadruplex by stacking with up two guanine bases [41], but this interaction produces only minimal variations in the SAXS curves. Indeed, high uncertainties characterize the Gibb's free energies derived for the MB binding processes (see **Table 1**), even if $\Delta G^0_{GMP} < \Delta G^0_{Gua}$. The slight preference of MB cations to bind to the negatively charged GMP with respect to the neutral Gua within the G-quadruplex structure is confirmed.

Table 1 Common fitting parameters of the SAXS analysis of Gua:GMP at different molar ratio and MB concentration.

κ	(a.u.)	5±2
v_K	(Å^3)	10.4±0.2
v_{GN}	(Å^3)	116±2
v_{RB}	(Å^3)	135±1
v_P	(Å^3)	30±2
v_{MB}	(Å^3)	360±20
v_W	(Å^3)	30.0±0.4
ΔG^0_{Gua}	(kJ/mol)	-20±10
ΔG^0_{GMP}	(kJ/mol)	-30±10

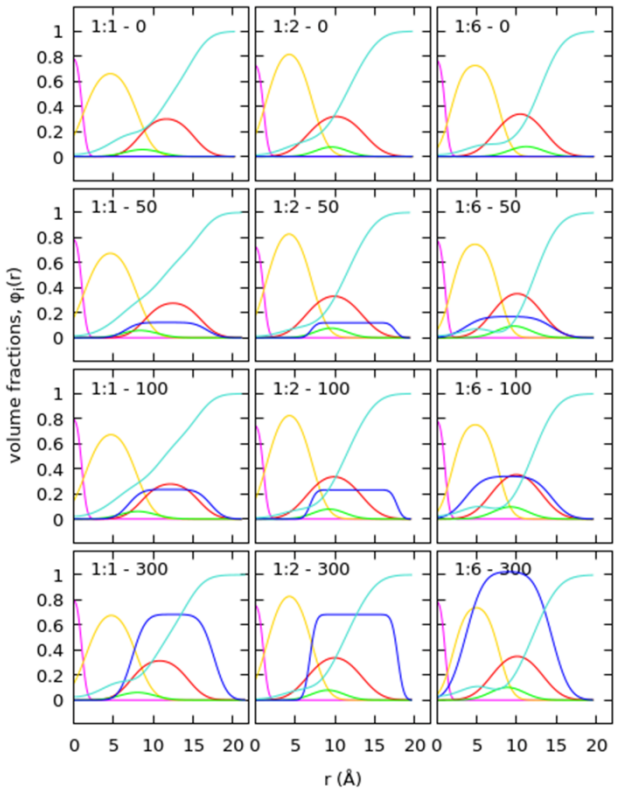

Figure 4. Volume fraction distributions, $\varphi_g(r)$, of the chemical groups derived from the analysis of SAXS data and plotted as a function of the distance r from the center of the G-tetramer. In each panel the Gua:GMP molar ratio and the concentration of MB (in μM unit) are reported. The colors refer to the following chemical groups: potassium cation (magenta), guanine (gold), ribose (red), phosphate (green), methylene blue (blue) and water (turquoise). Volume fractions of methylene blue are multiplied by a factor 600 for clarity.

3.2.2 Rheological measurements

Measurements of rheological parameters, such as elastic modulus (G'), viscous modulus (G''), and viscosity (η), as a function of frequency sweep and temperature were performed to obtain information regarding the viscoelastic properties of G-hydrogels.

The three drug-free samples (Gua:GMP = 1:1, 1:2 and 1:6) presented the elastic modulus values (G') higher than the viscous ones (G'') over the entire range of investigated frequency, indicating that the three formulations display a viscoelastic behavior (**Figure 5a**). On frequency sweep analysis, note that G' values are relatively low (between 10 and 100 Pa), in good agreement with other reported G-quadruplex-

based hydrogels [33,70,71], once the 3D network is simple due to the spontaneous G-wires entanglement. Higher G' values were found to Gua:GMP ratio 1:1 and 1:2, indicating higher strength of theses gels compared to the 1:6. Hence the hydrogel cohesion is an inversely GMP-proportion dependent process (**Figure 5a**).

The G' values were systematically decreased when MB was encapsulated into the three samples (**Figure 5a,b**). Therefore, the strength of the gels diminishes, probably due to the interaction between MB and G-quartets (especially with GMP residues), as inferred here by SAXS and docking simulations elsewhere [41]. The hydrogel Gua:GMP 1:6 presented a more pronounced change mainly at low frequencies and temperature, once this sample has the highest proportion of GMP which may favor the MB interaction compared to the others with lower GMP content (**Figure 5b**).

Regarding temperature sweep analysis, the behaviors of the elastic modulus of the 1:1 and 1:2 Gua:GMP hydrogels are similar at low-temperature range (from 0 to 30 °C). An abrupt decrease in G' curve for Gua:GMP 1:1 hydrogel can be appreciated in **Figure 5c**. Indeed, at 62.3 °C (inflection point indicated by the arrow in **Figure 5c**), the occurrence of the gel-sol phase temperature transition ($T_{gel\text{-}sol}$) must be associated to the hydrogels network disordering due to high temperatures. For Gua:GMP 1:2 hydrogel $T_{gel\text{-}sol}$ is 58.2 °C (**Figure 5c**), highlighting the fact that the 1:1 gel is more thermo-stable than 1:2 gel. The temperature scanning for the 1:6 hydrogel shows a plateau from 0 to 25 °C and a discrete peak with a maximum at 30 °C. Thenceforth, the G' values start to diminish due to the gel-sol phase transition at 47.5 °C, confirming this hydrogel is less resistant to temperature rise (**Figure 5c**). Similar results were previously detected by SAXS [18]; however, the step increment in temperature for SAXS measurements was 5 °C. Hence, the resolution in $T_{gel\text{-}sol}$ was impaired in that case. The $T_{gel\text{-}sol}$ values

determined by SAXS were approximately 70 °C, 65 °C and 45°C to 1:1, 1:2 and 1:6 hydrogels, respectively [18].

The temperature scanning for the MB-loaded hydrogels (100 μM of MB) showed that the $T_{gel-sol}$ were 62.2 °C, 57.4 °C, and 45.5 °C for the 1:1, 1:2, and 1:6 samples, respectively (**Figure 5d, Table 2**). The difference of $T_{gel-sol}$ between MB-loaded and MB-free hydrogels is 0.1; 0.8 and 2.0 °C for 1:1, 1:2, and 1:6, respectively, suggesting that MB affects the hydrogels thermal stability in a more pronounced extent as higher is the GMP proportion, since MB may interact more strongly to GMP than Gua, as proposed above by SAXS analysis.

It is worth mentioning that the temperature-dependent viscosity (η) values (**Table 2**) were found in the range from 0.025 to 6.8 Pa.s. A significant decrease in viscosity was observed from 40 to 50 °C for 1:6 sample. For the 1:2 hydrogel, the viscosity reduction occurred between 50 and 60 °C, while for the sample 1:1 the decrease was observed between 60 and 70 °C (**Table 2**), relating these viscosity decays to gel-sol transition.

The temperature-dependent feature and its influence on hydrogels viscosity are essential factors to be considered for biomedical applications, since the predominance of the storage (G') over the loss (G") modulus allows the modulation of the dissolution and drug release rates at physiological temperature. Besides, the hydrogels can be used as possible depot formulations, due to the network structural and cohesion maintenance at temperature intervals from 0 to 40 °C.

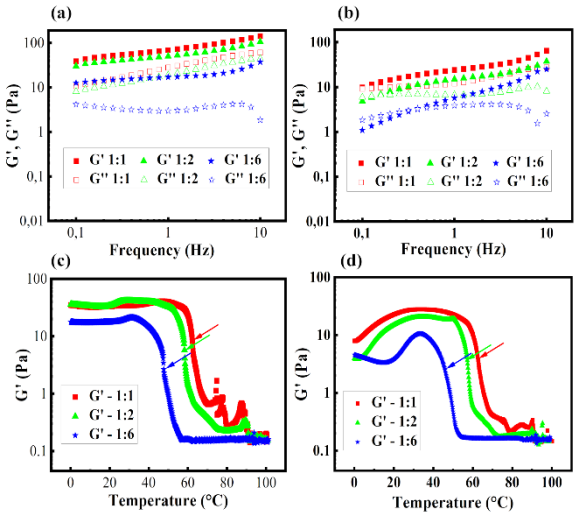

Figure 5. Rheological measurements of the three Gua:GMP hydrogels: 1:1 – red; 1:2 – green and 1:6 – blue (molar ratio) in presence and absence of MB. Rheograms for (a) MB-free and (b) MB-loaded, showing the dependency of elastic modulus - G' (filled symbols) and viscous modulus - G'' (empty symbols) with frequency sweep. Rheograms for (c) MB-free and (d) MB-loaded, showing the dependency of elastic modulus - G' with temperature scanning at constant frequency of 1Hz. The transition temperature from gel to sol phase ($T_{gel-sol}$) is 62.3 °C, 58.2 °C, and 47.2 °C for MB-free and 62.2 °C, 57.4 °C and 45.5 °C for MB-loaded 1:1, 1:2, and 1:6 samples, respectively, indicated by the arrows (inflection point).

Table 2 Temperature transition ($T_{gel-sol}$) and viscosity at different temperatures for the three hydrogels (Gua:GMP = 1:1, 1:2 and 1:6 molar ratio) in absence and presence of methylene blue ([MB] = 100 μM)

		MB-free hydrogels			**MB-loaded hydrogels**		
	Gua:GMP	**1:1**	**1:2**	**1:6**	**1:1**	**1:2**	**1:6**
	$T_{gel-sol}$ (ºC)	62.3	58.2	47.5	62.2	57.4	45.5
Temperature (ºC)		**Viscosity (mPa s)**			**Viscosity (mPa s)**		
40		6453	6782	2413	5011	3471	1383
50		6780	5426	208	4339	3520	136
60		4223	291	26	2411	128	26
70		121	66	25	86	38	25

3.3 Cell viability assessment

Toxicity of Gua:GMP hydrogels was analyzed by *in vitro* cell culture experiments. Two different methodologies were carried out to investigate cell viability in the presence of the hydrogels. In the first, the hydrogel was diluted into the cell

culture medium at different concentrations. In contrast, in the second, the hydrogel was firstly deposited in the well of the plate and then the cells were added and cultured on its surface. Microphotographs, optical, and fluorescence microscopy images were taken for both assays.

The first experiment (see results in **Figure 6a,b**) shows that the presence of hydrogel in different concentrations does not affect cell survival. Thus, the hydrogel seems biocompatible and suitable for biomedical applications. To verify whether higher hydrogel concentrations can affect cell survival, cells were deposited on the surface of pure hydrogels, and viability was assessed. Survival, as demonstrated by the presence of neutral red staining inside the cells, was observed in all cases. Still, a tendency to cell aggregation, more pronounced in the samples 1:1 and 1:2, was found in all groups (see **Figure 6c**). This probably happens because the G-hydrogel does not offer Arg-Gly-Asp (RGD) motifs that are required for cell-surface adhesion, thus aggregation occurs instead of adherence and proliferation. Nevertheless, the assay showed that, despite the aggregation, cells are mostly alive (one example is shown in **Figure S4** in the SM). An application seems immediately possible: G-hydrogels can be used to produce spheroid and tumor cell models as low adherence support. Recently, low adherence of G-quadruplex hydrogel was already detected [72]. In this case, the substrate for the cell culture was made by using G-quadruplexes as cross-linking points of poly(ethylene glycol) (PEG) [72].

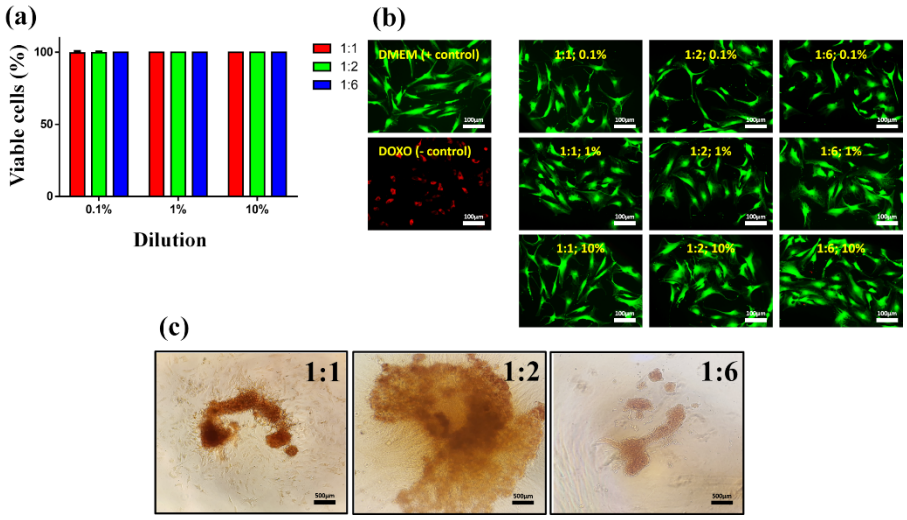

Figure 6. Cell viability assays of the three Gua:GMP hydrogels (1:1, 1:2 and 1:6) (a) Viable human adipose tissue-derived stromal cells (ASC) at different concentrations of hydrogels in the cell culture medium. (b) Fluorescent microscopy images from Live/Dead assay: green represents cells alive, and dead cells are stained in red (scale bar: 100µm). (c) Microphotography images from the cell culture using human adipose tissue-derived stromal cells (ASC) on the hydrogels surfaces stained with neutral red dye. The Gua:GMP ratios are indicated in the figure (scale bar: 500µm).

3.4 Penetration into and release of MB from the hydrogel matrix

3.4.1 Penetration of MB into the hydrogel matrix

The capability of the G-based hydrogels to trap and release bio-relevant molecules has been studied. The MB diffusion into the gel has been determined by placing an amount of 300 µM MB solution on the top of the hydrogel and letting it penetrate at neutral pH. Penetration is followed by visual inspection, obtaining the position of the front as a function of time by photographic registration (**Figure 7a**). The MB diffusion average rate was 13 µm min^{-1}, 20 µm $min^{-1,}$ and 30 µm min^{-1} for 1:1, 1:2, and 1:6, respectively. The MB reached the bottom of the vial after 270 minutes in the 1:6 hydrogel, while the total diffusion down to the base took 390 and 600 minutes for the 1:2 and 1:1 sample, respectively (**Figure 7b**), confirming the different microscopic entanglement of the different hydrogels. Note that in all cases, the hydrogel maintains stable and transparent.

For comparison purposes, similar experiments were performed using cytochrome C (CytC), a globular and soluble protein (12,000 MW and 40 Å diameter *vs.* 320 MW and 14 Å length for MB) (**Figure 7b**)**.** Noteworthy, the diffusion of CytC into the hydrogel matrix is much slower than that of MB, with average diffusion rate of 1.1 µm min^{-1}, 0.5 µm min^{-1} and 0.3 µm min^{-1}, requiring 120, 240, and 430 hours to reach the vial base for 1:6, 1:2 and 1:1 Gua:GMP hydrogels, respectively. Moreover, after penetration, the 1:1 Gua:GMP sample was not macroscopically homogeneous **Figure 7c**. Such results confirm that the difficulty in loading external molecules into the hydrogels depends on the entanglement of G-quadruplexes: mesh spaces may be big enough to allow diffusion. However, a large molecule cannot be able to access the entire matrix. Indeed, instead of being homogeneously distributed, CytC can thus accumulate in some regions, while other parts are almost CytC-free. Note indeed that SAXS profile of CytC-loaded 1:1 hydrogels presented an intensity increase at very low *Q*, indicating a possible protein aggregation, which was not observed for CytC-loaded 1:2 and 1:6 hydrogels (data not shown). When the hydrogel presents a looser interlacing with a more expanded mesh, the molecule diffusion and its distribution inside the matrix can be facilitated. Therefore, these results support the idea that the formulation of the G-hydrogel handling the proportion between Gua and GMP can be chosen depending on the molecule features to be encapsulated.

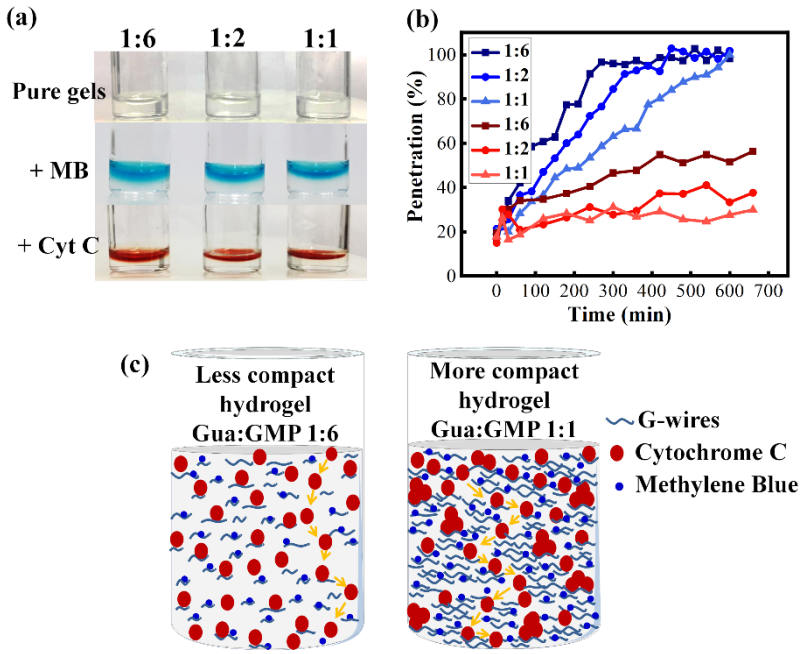

Figure 7. Drug penetration into Gua:GMP hydrogels matrix (a) Photographs of the drug diffusion after one hour of the experiment. (b) Percentage of Methylene Blue (blue) and Cytochrome C (red) penetration over time into hydrogel matrix, at neutral pH and room temperature. (c) A simplified 2D illustration representing a soft (like Gua:GMP = 1:6) and hard hydrogel (like Gua:GMP = 1:1). The diffusion of CytC (red circles) is represented by the yellow arrows.

3.4.2 In vitro MB release from hydrogels

As G-hydrogels are excellent candidates as drug delivery systems [2,65,67,73–81] we have evaluated the MB release from the gel matrix and, as suggested by the swelling test, their pH-responsiveness. Two methodologies of release were considered as follows.

3.4.2.1 In vitro drug release across the artificial membrane:

MB release from the three different hydrogels (1:6, 1:2, and 1:1) loaded with 100 µM of the drug was followed using the vertical Franz-type cells. The amount of MB released was monitored as a function of time by UV/Vis spectroscopy measuring the absorbance at λ = 665 nm, and results are shown in **Figure 8a**. Although the interaction with G-quadruplexes is rather strong, as indicated by SAXS, the amount of released MB was between 80 and 90% in 24 hours. It should be observed that the cumulative release

profile (**Figure 8a**) suggests that the mechanism is probably dependent on the hydrogel composition: in the first 8 hours, the amount of MB released is higher for the 1:6 sample (57%), followed by the 1:2 hydrogel (46%) and finally the 1:1 (31%), but the total amount of MB released from the 1:6 hydrogel after 24 hours was lower. The explanation can be attributed to the highest negative charge in this hydrogel (highest GMP proportion), which can sequester some MB molecules (positively charged) due to strong electrostatic interaction (see the different ΔGs in **Table 1**).

MB release from such matrices can be controlled either by solute diffusion and/or hydrogel dissolution: therefore, the cumulative release curves were analyzed considering the corresponding diffusion models. Results reported in **Table 3** reveal distinct mechanisms of MB release from the G-hydrogels. The best fitting of the 1:1 release curves indicates the Zero-order mechanism as the one with the highest correlation coefficient (R^2 = 0.999): MB diffusion from the matrix to the medium is predominant, probably because the high mechanical stability detected for this gel. Consequently, this hydrogel presents a more sustained and constant release. The other two hydrogels (1:6 and 1:2) follow the Korsmeyer-Peppas mechanism, based on a combination of both diffusion and erosion (R^2 = 0.9689 and 0.9402, for 1:6 and 1:2, respectively). In good agreement with the swelling and the mechanical properties of the different hydrogels (1:6 and 1:2 hydrogels are softer compared to the hard gel formed by 1:1 Gua:GMP), results suggest that the system hydration causes fast erosion, leading to a fast drug diffusion from the matrix to the release medium. Accordingly, K_{rel} (1:1) < K_{rel} (1:2) < K_{rel} (1:6) (**Table 3**).

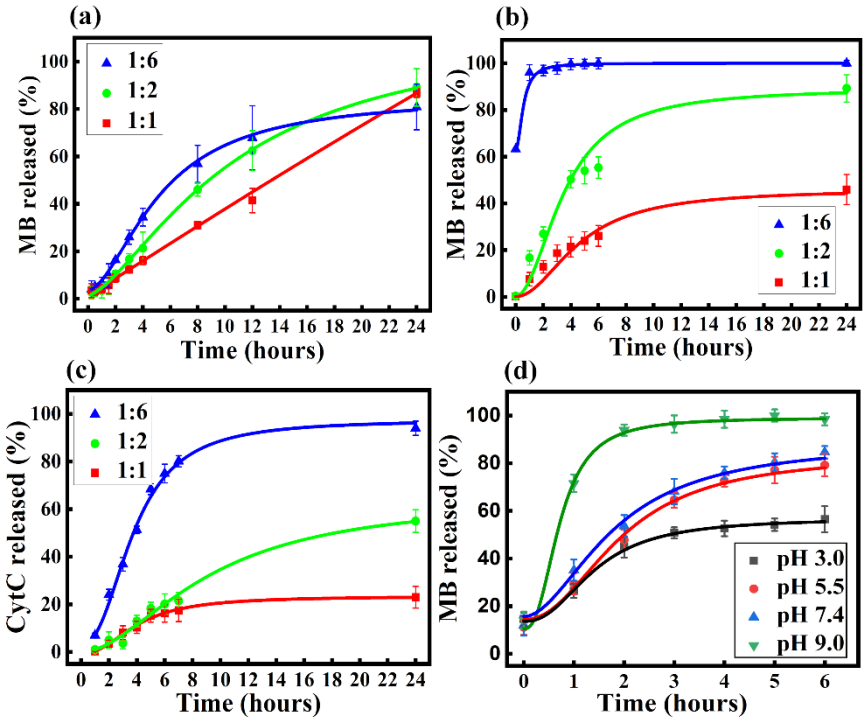

Figure 8. Drugs release profiles from Gua:GMP hydrogel matrix (a) Cumulative MB released from the hydrogels, at neutral pH, using the membrane diffusion model in vertical Franz-type cells. (b) MB and (c) CytC releases profiles from the hydrogels at neutral pH, using the dissolution system (hydrogel in direct contact with the receptor medium). Different Gua:GMP ratio-are represented by the colors: blue -1:6, green - 1:2, and red - 1:1. (d) MB release profile from the 1:2 hydrogel placed in mediums with different pHs: black - 3.0, red - 5.5, blue - 7.4, and green - 9.0. All measurements were carried out in triplicate, and averaged values are displayed. The error bars considered the minimum and maximum measured values.

Table 3 Parameters of the mathematical analysis of the curves of MB release from the hydrogel formed by different Gua:GMP ratio (1:6, 1:2, and 1:1) at neutral pH, using the membrane diffusion in vertical Franz-type cells, for three models: Zero-order, Higuchi, and Korsmeyer-Peppas

Formulations	**Zero-order**		**Higuchi**		**Korsmeyer–Peppas**		
	K_0(hour^{-1})	R^2	K_H (hour$^{-1/2}$)	R^2	K_{KP} (hour^{-n})	R^2	n
1:6	4.66	0.7898	18.5	0.9334	8.99	0.9689	0.804
1:2	4.62	0.9385	19.5	0.9273	5.56	0.9402	0.910
1:1	3.56	0.9992	19.5	0.9303	5.13	0.9648	0.819

3.4.2.2 In-vitro dissolution assays:

A membraneless method was also considered to evaluate the drug release in the case of direct contact of the hydrogel with the dissolution medium. As already observed, the three samples presented different swelling behaviors and then are characterized by a different drug release behavior. **Figure 8b** shows that the 1:1 hydrogel has the lowest release rate (K_{rel} = 2.73 $hour^{-1}$) (**Table S1** in the SM), and only 40% of loaded MB is released after 24 hours. An intermediate release rate is observed for 1:2 sample (K_{rel} =5.75 $hour^{-1}$) (**Table S1**), which is able to release the 85 % of MB after 24 hours. As the 1:6 hydrogel was rapidly disrupted in contact with water (**Figure 1a**), the MB release rate was not determined: the MB was totally released in 2 hours (**Figure 8b**).

Comparative experiments were performed on hydrogels loaded with Cytochrome C (note that while MB intercalates into G-quartets, CytC is dissolved in the aqueous compartment of the matrix). **Figure 8c** shows that only a small amount of CytC is released from 1:1 hydrogel (~ 20% after 24 hours) with K_{rel} = 1.40 $hour^{-1}$ (**Table S2** in the SM), while a release of 80 % of CytC has been obtained after 8 hours from the softest hydrogel (1:6) with K_{rel} = 5.62 $hour^{-1}$. As expected, the 1:2 hydrogel shows an intermediate behavior, with K_{rel} = 2.62 $hour^{-1}$ and 55% of protein released after 24 hours.

The MB release from G-hydrogels was also studied as a function of the environmental pH, e.g., as a function of the charge density of the G-quadruplexes, which dictates the level of cohesion of the gel matrix. The *in-vitro* dissolution assay was performed on the hydrogel 1:2, at pH changing from 3.0 to 9.0. As expected, the drug release was dependent on the pH of the medium: at low pH (3.0), the formation of a tighter gel enhanced the MB entrapment, resulting in a low release rate (K_{rel} = 7.78 $hour^{-1}$) (**Figure 8d, Table S3**). By increasing the pH, the MB release was higher, and no differences were detected between pH 5.5 and 7.4 (K_{rel} = 12.3 $hour^{-1}$) (**Table S3**).

Interesting, the behavior was substantially similar to the one seen before, in neutral pH, suggesting that the entanglement of the fibers is kept the same. The pH increment to 9.0 enhances the G-quadruplex-G-quadruplex repulsion, and the matrix becomes less compact, promoting the release of practically all MB during the first hour (**Figure 8d**). In summary, 1:2 sample behaves as 1:1 Gua:GMP hydrogel at low pH and is more similar to 1:6 hydrogel in an alkaline medium.

4. Conclusion

In this work, we reported that different molar ratio between Gua and GMP can be tailored to produce self-assembled hydrogels with a similar structural organization but different microscopic and macroscopic properties. Such soft materials present relevant features such as stability, swelling, self-healing, stretchiness, flexibility, and pH responsiveness which can be useful to produce drug delivery systems. The main parameters responsible for the modulation of G-hydrogel properties are the number of negative charges along the G-quadruplexes, due to the phosphate groups of GMP, and the localized attraction between their Gua-rich regions. Therefore, any changes in composition and pH of the medium appear as modulator factors tuning hydrogel stability, softness, erosion and swelling. Accordingly, G-hydrogel mechanical properties modulate the rate of diffusion and the mechanism of MB release. Noticeable, comparative experiments with CytC suggest that the features of the loaded molecule could also modify drug loading and release.

Therefore, the combined results give us support to conclude that the self-assembled Gua:GMP hydrogels are non-toxic, being promising candidates to be applied as drug-delivery systems, to entrap and deliver therapeutics in a sustained release manner and pH responsiveness. In particular, we show that MB-loaded Gua-GMP

hydrogels have interesting features to be potentially employed as PS-encapsulating novel biomaterial. Further studies are required to determine its efficiency in antimicrobial and photodynamic therapy. Moreover, the current work paves the way of designing novel G-based hydrogels able to entrap and release key proteins for biotechnological and biomedical applications.

CRediT authorship contribution statement

J.S. Yoneda: Conceptualization, Formal analysis, Investigation, Writing - original draft. **D.R. de Araújo**: Conceptualization, Formal analysis, Investigation, Resources, Writing - original draft. **F. Sella**: Investigation. **G.R. Liguori**: Investigation. **T.T.A. Liguori** : Investigation. **L.F.P. Moreira** : Investigation, Resources. **F. Spinozzi** : Formal analysis, Writing - original draft. **P. Mariani**: Conceptualization, Formal analysis, Writing - original draft. **R. Itri**: Conceptualization, Resources, Writing - original draft, Supervision, Funding acquisition.

Declaration of Competing Interest

The authors declare that they have no known competing financial interests or personal relationships that could have appeared to influence the work reported in this paper.

Acknowledgments

The authors wish to thank to São Paulo Research Foundation (FAPESP), CNPq and CAPES for the financial support. Juliana Sakamoto Yoneda acknowledges FAPESP for the Post-Doctoral fellowship process number 2018/07194-9. R. Itri is recipient from

CNPq research fellowship, D.R. de Araújo is recipient from CNPq research fellowship (307718/2019-0).

The authors thank to Ivana A. Borin of the Laboratory of Atomic Force Microscopy of the Chemistry Department – FFCLRP – USP (Brazil) for AFM measurements and to Antonio Carlos Franco and Társis Mendes Germano for the support in X-ray measurements.

Supplementary material

The photographs of the hydrogels during the swelling experiment, the X-Ray diffraction (XRD) showing the fingerprint for G-quartets stacking, the total electron density and contribution of each group derived from SAXS analysis, the phase contrast, and fluorescent microscopy images from Live/Dead assay of ASC cultured on the surface of the hydrogel, and the tables with parameters for the drug release tests.

References

[1] A.P. Mathew, S. Uthaman, K.H. Cho, C.S. Cho, I.K. Park, Injectable hydrogels for delivering biotherapeutic molecules, Int. J. Biol. Macromol. 110 (2018) 17–29. https://doi.org/10.1016/j.ijbiomac.2017.11.113.

[2] T. Thambi, Y. Li, D.S. Lee, Injectable hydrogels for sustained release of therapeutic agents, J. Control. Release. 267 (2017) 57–66. https://doi.org/10.1016/j.jconrel.2017.08.006.

[3] Y.N. Wang, C.K. Adokoh, R. Narain, Recent development and biomedical applications of self-healing hydrogels, Expert Opin. Drug Deliv. 15 (2018) 77–91. https://doi.org/10.1080/17425247.2017.1360865.

[4] I.Y. Jung, J.S. Kim, B.R. Choi, K. Lee, H. Lee, Hydrogel Based Biosensors for In Vitro Diagnostics of Biochemicals, Proteins, and Genes, Adv Heal. Mater. 6 (2017). https://doi.org/10.1002/adhm.201601475.

[5] J.H. Lee, Injectable hydrogels delivering therapeutic agents for disease treatment and tissue engineering, Biomater Res. 22 (2018) 27. https://doi.org/10.1186/s40824-018-0138-6.

[6] K.J. Skilling, F. Citossi, T.D. Bradshaw, M. Ashford, B. Kellam, M. Marlow, Insights into low molecular mass organic gelators: a focus on drug delivery and tissue engineering applications, Soft Matter. 10 (2014) 237–256. https://doi.org/10.1039/c3sm52244j.

[7] E.R. Draper, D.J. Adams, Low-Molecular-Weight Gels: The State of the Art, Chem. 3 (2017) 390–410. https://doi.org/10.1016/j.chempr.2017.07.012.

[8] S. Xiao, J.T. Davis, G4-quartet hydrogels from 5′-hydrazino-guanosine for the non-covalent and covalent remediation of contaminants from water, Faraday Discuss. 209 (2018) 97–112. https://doi.org/10.1039/c8fd00038g.

[9] X. Du, J. Zhou, J. Shi, B. Xu, Supramolecular Hydrogelators and Hydrogels: From Soft Matter to Molecular Biomaterials, Chem Rev. 115 (2015) 13165–13307. https://doi.org/10.1021/acs.chemrev.5b00299.

[10] X. Hu, Y. Wang, L. Zhang, M. Xu, Construction of self-assembled polyelectrolyte complex hydrogel based on oppositely charged polysaccharides for sustained delivery of green tea polyphenols, Food Chem. (2020). https://doi.org/10.1016/j.foodchem.2019.125632.

[11] X. Hu, Y. Wang, L. Zhang, M. Xu, Formation of self-assembled polyelectrolyte complex hydrogel derived from salecan and chitosan for sustained release of Vitamin C, Carbohydr. Polym. (2020).

https://doi.org/10.1016/j.carbpol.2020.115920.

[12] X. Hu, L. Yan, Y. Wang, M. Xu, Self-assembly of binary oppositely charged polysaccharides into polyelectrolyte complex hydrogel film for facile and efficient Pb2+ removal, Chem. Eng. J. (2020). https://doi.org/10.1016/j.cej.2020.124189.

[13] X. Hu, L. Yan, Y. Wang, M. Xu, Freeze-thaw as a route to build manageable polysaccharide cryogel for deep cleaning of crystal violet, Chem. Eng. J. (2020). https://doi.org/10.1016/j.cej.2020.125354.

[14] J.M. Knipe, N.A. Peppas, Multi-responsive hydrogels for drug delivery and tissue engineering applications, Regen Biomater. 1 (2014) 57–65. https://doi.org/10.1093/rb/rbu006.

[15] S. Tanaka, K. Wakabayashi, K. Fukushima, S. Yukami, R. Maezawa, Y. Takeda, K. Tatsumi, Y. Ohya, A. Kuzuya, Intelligent, Biodegradable, and Self-Healing Hydrogels Utilizing DNA Quadruplexes, Chem. Asian J. 12 (2017) 2388–2392. https://doi.org/10.1002/asia.201701066.

[16] X.Y. Bai, Z.X. Bao, S.C. Bi, Y. Li, X.P. Yu, S.H. Hu, M.P. Tian, X. Zhang, X.J. Cheng, X.G. Chen, Chitosan-Based Thermo/pH Double Sensitive Hydrogel for Controlled Drug Delivery, Macromol. Biosci. 18 (2018). https://doi.org/10.1002/mabi.201700305.

[17] M.H. Turabee, T. Thambi, H. Duong, J.H. Jeong, D.S. Lee, A pH- and temperature-responsive bioresorbable injectable hydrogel based on polypeptide block copolymers for the sustained delivery of proteins in vivo, Biomater. Sci. 6 (2018) 661–671. https://doi.org/10.1039/c7bm00980a.

[18] F. Carducci, J.S. Yoneda, R. Itri, P. Mariani, On the structural stability of guanosine-based supramolecular hydrogels, Soft Matter. 14 (2018) 2938–2948.

https://doi.org/10.1039/C8SM00299A.

[19] T. Bhattacharyya, P. Saha, J. Dash, Guanosine-Derived Supramolecular Hydrogels: Recent Developments and Future Opportunities, Acs Omega. 3 (2018) 2230–2241. https://doi.org/10.1021/acsomega.7b02039.

[20] M. Chen, W.M. Lin, L. Hong, N. Ji, H. Zhao, The Development and Lifetime Stability Improvement of Guanosine-Based Supramolecular Hydrogels through Optimized Structure, Biomed Res. Int. (2019). https://doi.org/10.1155/2019/6258248.

[21] G.M. Peters, J.T. Davis, Supramolecular gels made from nucleobase, nucleoside and nucleotide analogs, Chem. Soc. Rev. 45 (2016) 3188–3206. https://doi.org/10.1039/c6cs00183a.

[22] V. Abet, R. Rodriguez, Guanosine and isoguanosine derivatives for supramolecular devices, New J. Chem. 38 (2014) 5122–5128. https://doi.org/10.1039/c4nj00665h.

[23] G.M. Peters, L.P. Skala, T.N. Plank, B.J. Hyman, G.N.M. Reddy, A. Marsh, S.P. Brown, J.T. Davis, A G(4)center dot K+ Hydrogel Stabilized by an Anion, J. Am. Chem. Soc. 136 (2014) 12596–12599. https://doi.org/10.1021/ja507506c.

[24] P. Mariani, F. Spinozzi, F. Federiconi, M.G. Ortore, H. Amenitsch, L. Spindler, I. Drevensek-Olenik, Guanosine quadruplexes in solution: a small-angle x-ray scattering analysis of temperature effects on self-assembling of deoxyguanosine monophosphate, J Nucleic Acids. 2010 (2010) 472478. https://doi.org/10.4061/2010/472478.

[25] J.T. Davis, G-quartets 40 years later: from 5’-GMP to molecular biology and supramolecular chemistry, Angew Chem Int Ed Engl. 43 (2004) 668–698. https://doi.org/10.1002/anie.200300589.

[26] L. Stefan, D. Monchaud, Applications of guanine quartets in nanotechnology and chemical biology, Nat. Rev. Chem. 3 (2019) 650–668. https://doi.org/10.1038/s41570-019-0132-0.

[27] S. Pieraccini, M. Campitiello, F. Carducci, J.T. Davis, P. Mariani, S. Masiero, Playing supramolecular dominoes with light: building and breaking a photoreversible G-quadruplex made from guanosine, boric acid and an azobenzene, Org Biomol Chem. 17 (2019) 2759–2769. https://doi.org/10.1039/c9ob00193j.

[28] J.E. Baldassarri, G.M. Ortore, F. Spinozzi, A. Round, C. Ferrero, P. Mariani, K vs. Na Effects on the Self-Assembly of Guanosine 5'-Monophosphate: A Solution SAXS Structural Study, Nanomaterials. 10 (2020) 629. https://doi.org/10.3390/nano10040629.

[29] H. Zhao, A. Schafer, F. Seela, Supramolecular Isoguanosine Assemblies Form Hydrogels with Excellent Long-Term Stability, Chempluschem. 82 (2017) 813. https://doi.org/10.1002/cplu.201700118.

[30] T.N. Plank, L.P. Skala, J.T. Davis, Supramolecular hydrogels for environmental remediation: G(4)-quartet gels that selectively absorb anionic dyes from water, Chem. Commun. 53 (2017) 6235–6238. https://doi.org/10.1039/c7cc03118a.

[31] J. Zhang, X.Y. Li, X.P. Sun, A.X. Song, Y.B. Tan, J.C. Hao, GMP-quadruplex-based hydrogels stabilized by lanthanide ions, Sci. China-Chemistry. 61 (2018) 604–612. https://doi.org/10.1007/s11426-017-9187-x.

[32] R. Belda, E. García-España, G.A. Morris, J.W. Steed, J.A. Aguilar, Guanosine-5'-Monophosphate Polyamine Hybrid Hydrogels: Enhanced Gel Strength Probed by z-Spectroscopy, Chemistry (Easton). 23 (2017) 7755–7760. https://doi.org/10.1002/chem.201700642.

[33] H. Feng, Y. Du, F. Tang, N. Ji, X. Zhao, H. Zhao, Q. Chen, Silver ions blocking crystallization of guanosine-based hydrogel for potential antimicrobial applications, RSC Adv. 8 (2018) 15842–15852. https://doi.org/10.1039/C8RA02500B.

[34] Y. Yu, V.L. Pushparaj, O. Nalamasu, L.B. McGown, G-quadruplex guanosine gels and single walled carbon nanotubes, Molecules. 18 (2013) 15434–15447. https://doi.org/10.3390/molecules181215434.

[35] Y. Yu, D. Nakamura, K. DeBoyace, A.W. Neisius, L.B. McGown, Tunable thermoassociation of binary guanosine gels, J. Phys. Chem. B. 112 (2008) 1130–1134. https://doi.org/10.1021/jp709613p.

[36] G. Nava, F. Carducci, R. Itri, J.S. Yoneda, T. Bellini, P. Mariani, Quadruplex knots as network nodes: nano-partitioning of guanosine derivates in supramolecular hydrogels, Soft Matter. 15 (2019) 2315–2318. https://doi.org/10.1039/c8sm02616e.

[37] E.M. Tuite, J.M. Kelly, Photochemical interactions of methylene blue and analogues with DNA and other biological substrates, J Photochem Photobiol B. (1993).

[38] M. Ortiz, A. Fragoso, P.J. Ortiz, C.K. O'Sullivan, Elucidation of the mechanism of single-stranded DNA interaction with methylene blue: A spectroscopic approach, J. Photochem. Photobiol. A Chem. (2011). https://doi.org/10.1016/j.jphotochem.2010.11.020.

[39] E. Farjami, L. Clima, K. V. Gothelf, E.E. Ferapontova, DNA interactions with a Methylene Blue redox indicator depend on the DNA length and are sequence specific, Analyst. (2010). https://doi.org/10.1039/c0an00049c.

[40] F.T. Zhang, J. Nie, D.W. Zhang, J.T. Chen, Y.L. Zhou, X.X. Zhang, Methylene

Blue as a G-Quadruplex Binding Probe for Label-Free Homogeneous Electrochemical Biosensing, Anal. Chem. 86 (2014) 9489–9495. https://doi.org/10.1021/ac502540m.

[41] T. Cao, F.T. Zhang, L.Y. Cai, Y.L. Zhou, N.J. Buurma, X.X. Zhang, Investigation of the interactions between methylene blue and intramolecular G-quadruplexes: an explicit distinction in electrochemical behavior, Analyst. 142 (2017) 987–993. https://doi.org/10.1039/c7an00083a.

[42] C.S. Foote, Mechanisms of photosensitized oxidation, Science (80-.). (1968). https://doi.org/10.1126/science.162.3857.963.

[43] D. Severino, H.C. Junqueira, M. Gugliotti, D.S. Gabrielli, M.S. Baptista, Influence of Negatively Charged Interfaces on the Ground and Excited State Properties of Methylene Blue¶, Photochem. Photobiol. (2003). https://doi.org/10.1562/0031-8655(2003)077<0459:ioncio>2.0.co;2.

[44] D. Gabrielli, E. Belisle, D. Severino, A.J. Kowaltowski, M.S. Baptista, Binding, Aggregation and Photochemical Properties of Methylene Blue in Mitochondrial Suspensions, Photochem. Photobiol. (2004). https://doi.org/10.1562/be-03-27.1.

[45] J.P. Tardivo, A. Del Giglio, C.S. De Oliveira, D.S. Gabrielli, H.C. Junqueira, D.B. Tada, D. Severino, R. De Fátima Turchiello, M.S. Baptista, Methylene blue in photodynamic therapy: From basic mechanisms to clinical applications, Photodiagnosis Photodyn. Ther. (2005). https://doi.org/10.1016/S1572-1000(05)00097-9.

[46] J.P. Tardivo, F. Adami, J.A. Correa, M.A. parecid. S. Pinhal, M.S. Baptista, A clinical trial testing the efficacy of PDT in preventing amputation in diabetic patients, Photodiagnosis Photodyn. Ther. (2014). https://doi.org/10.1016/j.pdpdt.2014.04.007.

[47] O. Chiarelli-Neto, C. Pavani, A. S. Ferreira, A.F. Uchoa, D. Severino, M.S. Baptista, Generation and suppression of singlet oxygen in hair by photosensitization of melanin, Free Radic. Biol. Med. (2011). https://doi.org/10.1016/j.freeradbiomed.2011.06.013.

[48] A.F. dos Santos, L.F. Terra, R.A.M. Wailemann, T.C. Oliveira, V. de Morais Gomes, M.F. Mineiro, F.C. Meotti, A. Bruni-Cardoso, M.S. Baptista, L. Labriola, Methylene blue photodynamic therapy induces selective and massive cell death in human breast cancer cells, BMC Cancer. (2017). https://doi.org/10.1186/s12885-017-3179-7.

[49] L.Y. Xia, X. Zhang, M. Cao, Z. Chen, F.G. Wu, Enhanced Fluorescence Emission and Singlet Oxygen Generation of Photosensitizers Embedded in Injectable Hydrogels for Imaging-Guided Photodynamic Cancer Therapy, Biomacromolecules. (2017). https://doi.org/10.1021/acs.biomac.7b00725.

[50] J. Méndez, M. Morales Cruz, Y. Delgado, C.M. Figueroa, E.A. Orellano, M. Morales, A. Monteagudo, K. Griebenow, Delivery of chemically glycosylated cytochrome c immobilized in mesoporous silica nanoparticles induces apoptosis in HeLa cancer cells, Mol. Pharm. (2014). https://doi.org/10.1021/mp400400j.

[51] S. Santra, C. Kaittanis, J.M. Perez, Cytochrome c encapsulating theranostic nanoparticles: A novel bifunctional system for targeted delivery of therapeutic membrane-impermeable proteins to tumors and imaging of cancer therapy, Mol. Pharm. (2010). https://doi.org/10.1021/mp100043h.

[52] S.K. Kim, M.B. Foote, L. Huang, The targeted intracellular delivery of cytochrome C protein to tumors using lipid-apolipoprotein nanoparticles, Biomaterials. (2012). https://doi.org/10.1016/j.biomaterials.2012.02.010.

[53] T.H. Yeh, F.L.L. Wu, L.J. Shen, Intracellular delivery of cytochrome c by

galactosylated albumin to hepatocarcinoma cells, J. Drug Target. (2014). https://doi.org/10.3109/1061186X.2014.905947.

[54] J.S. Pedersen, P. Schurtenberger, Scattering Functions of Semiflexible Polymers with and without Excluded Volume Effects, Macromolecules. 29 (1996) 7602–7612. https://doi.org/- 10.1021/ma9607630.

[55] P. Mariani, L. Saturni, Measurement of intercolumnar forces between parallel guanosine four-stranded helices, Biophys J. 70 (1996) 2867–2874. https://doi.org/10.1016/S0006-3495(96)79856-9.

[56] P. Mariani, F. Ciuchi, L. Saturni, Helix-specific interactions induce condensation of guanosine four-stranded helices in concentrated salt solutions, Biophys J. 74 (1998) 430–435. https://doi.org/10.1016/S0006-3495(98)77800-2.

[57] F. Spinozzi, C. Ferrero, M.G. Ortore, A. De Maria Antolinos, P. Mariani, GENFIT: software for the analysis of small-angle X-ray and neutron scattering data of macro-molecules in solution, J Appl Crystallogr. 47 (2014) 1132–1139. https://doi.org/10.1107/S1600576714005147.

[58] C.L. Oliveira, M.A. Behrens, J.S. Pedersen, K. Erlacher, D. Otzen, A SAXS study of glucagon fibrillation, J Mol Biol. 387 (2009) 147–161. https://doi.org/10.1016/j.jmb.2009.01.020.

[59] J. Teixeira, Small-angle scattering by fractal systems, J. Appl. Crystallogr. 21 (1988) 781–785. https://doi.org/10.1107/S0021889888000263.

[60] T.T.A. Liguori, G.R. Liguori, L.F.P. Moreira, M.C. Harmsen, Fibroblast growth factor-2, but not the adipose tissue-derived stromal cells secretome, inhibits TGF-beta 1-induced differentiation of human cardiac fibroblasts into myofibroblasts, Sci. Rep. 8 (2018). https://doi.org/10.1038/s41598-018-34747-3.

[61] G.R. Liguori, Q. Zhou, T.T.A. Liguori, G.G. Barros, P.T. Kühn, L.F.P. Moreira,

P. van Rijn, M.C. Harmsen, Directional Topography Influences Adipose Mesenchymal Stromal Cell Plasticity: Prospects for Tissue Engineering and Fibrosis, Stem Cells Int. 2019 (2019) 5387850. https://doi.org/10.1155/2019/5387850.

[62] T.T.A. Liguori, G.R. Liguori, L.F.P. Moreira, M.C. Harmsen, Adipose tissue-derived stromal cells' conditioned medium modulates endothelial-mesenchymal transition induced by IL-1 beta/TGF-beta 2 but does not restore endothelial function, Cell Prolif. 52 (2019) e12629. https://doi.org/10.1111/cpr.12629.

[63] B. Adhikari, A. Shah, H.B. Kraatz, Self-assembly of guanosine and deoxy-guanosine into hydrogels: monovalent cation guided modulation of gelation, morphology and self-healing properties, J. Mater. Chem. B. 2 (2014) 4802–4810. https://doi.org/10.1039/c4tb00702f.

[64] F. Tang, H. Feng, Y.Q. Du, Y.D. Xiao, H.X. Dan, H. Zhao, Q.M. Chen, Developing a Self-Healing Supramolecular Nucleoside Hydrogel Based on Guanosine and Isoguanosine, Chem. Asian J. 13 (2018) 1962–1971. https://doi.org/10.1002/asia.201800788.

[65] H. Zhao, H. Feng, J. Liu, F. Tang, Y. Du, N. Ji, L. Xie, X. Zhao, Z. Wang, Q. Chen, Dual-functional guanosine-based hydrogel integrating localized delivery and anticancer activities for cancer therapy, Biomaterials. 230 (2020) 119598. https://doi.org/10.1016/j.biomaterials.2019.119598.

[66] S. Kumar, A. Bajaj, Advances in self-assembled injectable hydrogels for cancer therapy, Biomater Sci. 8 (2020) 2055. https://doi.org/10.1039/d0bm00146e.

[67] T. Ghosh, A. Biswas, P.K. Gavel, A.K. Das, Engineered Dynamic Boronate Ester-Mediated Self-Healable Biocompatible G-Quadruplex Hydrogels for Sustained Release of Vitamins, Langmuir. 36 (2020) 1574–1584.

https://doi.org/10.1021/acs.langmuir.9b03837.

[68] Y. Tu, N. Chen, C. Li, H. Liu, R. Zhu, S. Chen, Q. Xiao, J. Liu, S. Ramakrishna, L. He, Advances in injectable self-healing biomedical hydrogels, Acta Biomater. 90 (2019) 1–20. https://doi.org/10.1016/j.actbio.2019.03.057.

[69] S.J. Perkins, X-ray and Neutron Solution Scattering, Elsevier, 1988.

[70] X. Li, A. Sánchez-Ferrer, M. Bagnani, J. Adamcik, P. Azzari, J. Hao, A. Song, H. Liu, R. Mezzenga, Metal ions confinement defines the architecture of G-quartet, G-quadruplex fibrils and their assembly into nematic tactoids, Proc Natl Acad Sci U S A. 117 (2020) 9832–9839. https://doi.org/10.1073/pnas.1919777117.

[71] M.S. Xiao, L. Gao, A.R. Chandrasekarand, J.F. Zhao, Q. Tang, Z.B. Qu, F. Wang, L. Li, Y. Yang, X.L. Zhang, Y. Wa, H. Pei, Bio-functional G-molecular hydrogels for accelerated wound healing, Mater. Sci. Eng. C-Materials Biol. Appl. 105 (2019). https://doi.org/10.1016/j.msec.2019.110067.

[72] S. Tanaka, S. Yukami, Y. Hachiro, Y. Ohya, A. Kuzuya, Application of DNA Quadruplex Hydrogels Prepared from Polyethylene Glycol-Oligodeoxynucleotide Conjugates to Cell Culture Media, Polym. 11 (2019). https://doi.org/10.3390/polym11101607.

[73] V. Venkatesh, N.K. Mishra, I. Romero-Canelon, R.R. Vernooij, H.Y. Shi, J.P.C. Coverdale, A. Habtemariam, S. Verma, P.J. Sadler, Supramolecular Photoactivatable Anticancer Hydrogels, J. Am. Chem. Soc. 139 (2017) 5656–5659. https://doi.org/10.1021/jacs.7b00186.

[74] J. Hu, Q. Hu, X. He, C. Liu, Y. Kong, Y. Cheng, Y. Zhang, Stimuli-Responsive Hydrogels with Antibacterial Activity Assembled from Guanosine, Aminoglycoside, and a Bifunctional Anchor, Adv Heal. Mater. 9 (2020) e1901329. https://doi.org/10.1002/adhm.201901329.

[75] A. Chyzy, M. Tomczykowa, M.E. Plonska-Brzezinska, Hydrogels as Potential Nano-, Micro- and Macro-Scale Systems for Controlled Drug Delivery, Mater. 13 (2020). https://doi.org/10.3390/ma13010188.

[76] A. Biswas, T. Ghosh, P.K. Gavel, A.K. Das, PEG Functionalized Stimuli Responsive Self-Healable Injectable Dynamic Imino-boronate G-quadruplex Hydrogel for the Delivery of Doxorubicin, ACS Appl. Bio Mater. 3 (2020) 1052–1060. https://doi.org/10.1021/acsabm.9b01034.

[77] Y. Li, Y. Liu, R. Ma, Y. Xu, Y. Zhang, B. Li, Y. An, L. Shi, A G-Quadruplex Hydrogel via Multicomponent Self-Assembly: Formation and Zero-Order Controlled Release, ACS Appl Mater Interfaces. 9 (2017) 13056–13067. https://doi.org/10.1021/acsami.7b00957.

[78] S.C. Lee, I.K. Kwon, K. Park, Hydrogels for delivery of bioactive agents: a historical perspective, Adv Drug Deliv Rev. 65 (2013) 17–20. https://doi.org/10.1016/j.addr.2012.07.015.

[79] Y. Wang, Programmable hydrogels, Biomaterials. 178 (2018) 663–680. https://doi.org/10.1016/j.biomaterials.2018.03.008.

[80] R.N. Das, Y.P. Kumar, S. Pagoti, A.J. Patil, J. Dash, Diffusion and Birefringence of Bioactive Dyes in a Supramolecular Guanosine Hydrogel, Chem. Eur. J. 18 (2012) 6008–6014. https://doi.org/10.1002/chem.201103814.

[81] N. Sreenivasachary, J.M. Lehn, Structural selection in G-quartet-based hydrogels and controlled release of bioactive molecules, Chem. Asian J. 3 (2008) 134–139. https://doi.org/10.1002/asia.200700041.

Self-assembled Guanosine-hydrogels for Drug-delivery Application: Structural and Mechanical Characterization, Methylene Blue Loading and Controlled Release

Juliana S. Yoneda[*1†], Daniele R. de Araujo[2], Fiorenza Sella[3], Gabriel R. Liguori[4], Tácia T. A. Liguori[4], Luiz Felipe P. Moreira[4], Francesco Spinozzi[3], Paolo Mariani[3], Rosangela Itri*[*1]*

[1]Instituto de Fisica, Universidade de São Paulo, São Paulo, SP, Brazil;

[2]Universidade Federal do ABC, Santo André – Brazil;

[3]Dipartimento di Scienze della Vita e dell'Ambiente, Università Politecnica delle Marche, Ancona – Italy;

[4]Instituto do Coração (InCor), Hospital das Clinicas HCFMUSP, Faculdade de Medicina, Universidade de São Paulo, São Paulo, SP, BR.

* email corresponding authors: julianasakamoto@hotmail.com; itri@if.usp.br

Supplementary Material

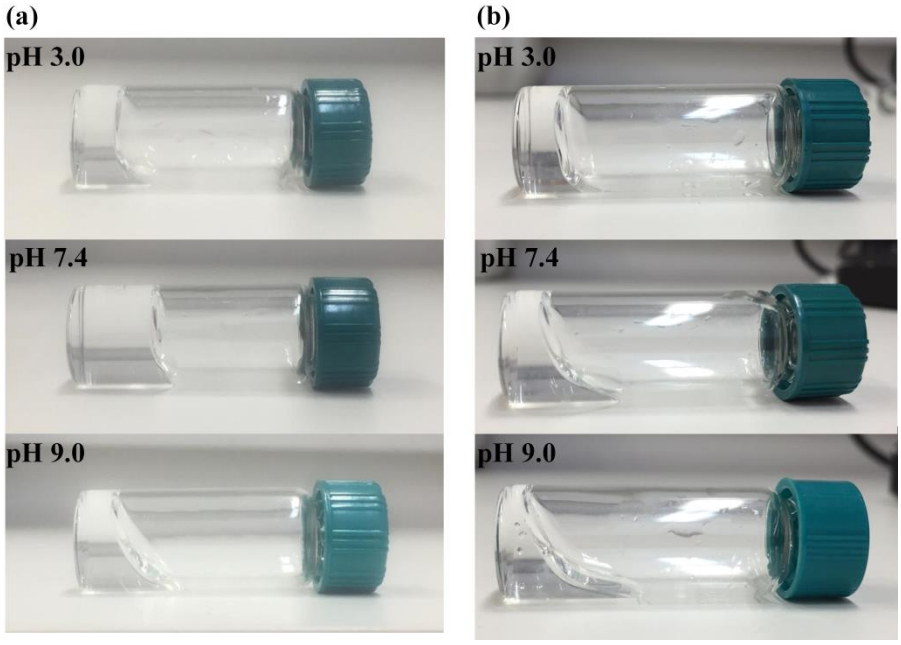

Figure S1. Photographs of the vials during the swelling experiment at different pHs indicated in the figure. (a) Gua:GMP 1:1 molar ratio after 140 h and (b) 1:2 molar ratio after 24 h.

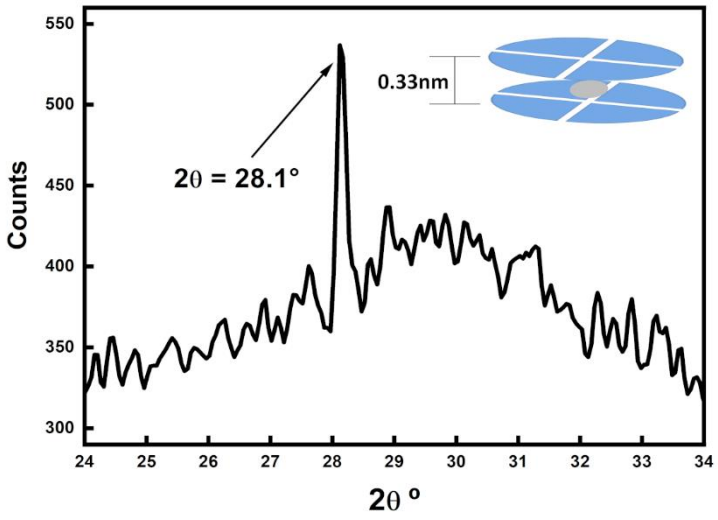

Figure S2: X-ray diffraction pattern of the Gua:GMP hydrogel. The peak is related to distance of the G-quartets inside the G-quadruplex fibers. For XRD, the hydrogel

sample were dried on the top of an acrylic sample holder and analyzed using a D8 Diffractometer (Bruker Corporation).

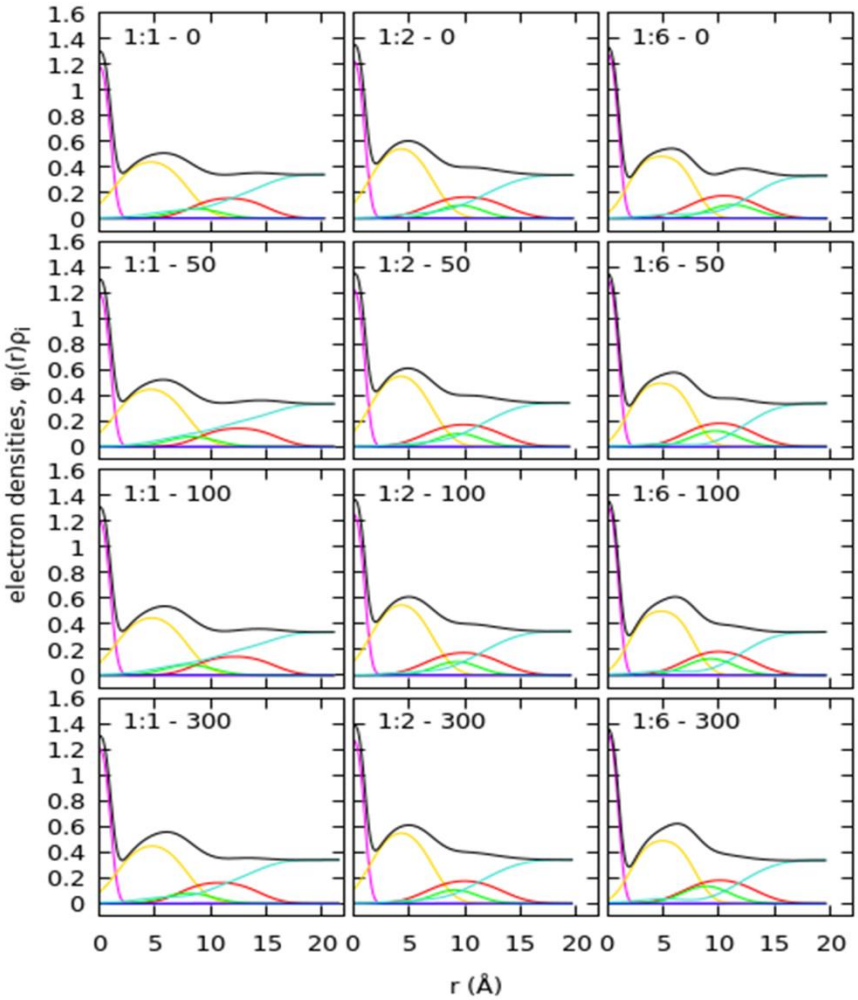

Figure S3. Total electron density (black lines) and contribution of each group: potassium cation (magenta), guanine (gold), ribose (red), phosphate (green), methylene blue (blue) and water (turquoise) in the hydrogels. Gua:GMP molar ratio and MB concentrations ranging from 0 to 300 μM are displayed in the figures.

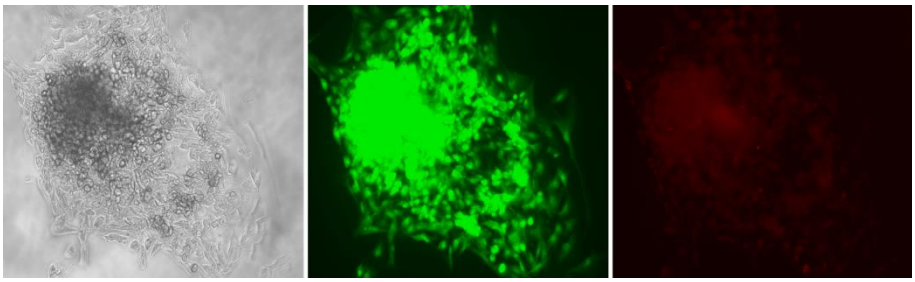

Figure S4. Left: Phase contrast and fluorescent microscopy images from Live/Dead assay (green represents cells alive – middle, and dead cells are stained in red - right) of human adipose tissue-derived stromal cells (ASC) cultured on the surface of the hydrogel Gua:GMP 1:2 molar ratio.

Table S1. Parameters of the mathematical analysis of the curves of MB release from the hydrogel formed by different Gua:GMP ratio (1:6, 1:2, and 1:1) at neutral pH, using the membraneless method for three models: Zero-order, Higuchi and Korsmeyer-Peppas

Formulations	**Zero-order**		**Higuchi**		**Korsmeyer–Peppas**		
	K_0(hour^{-1})	R^2	K_H (hour$^{-1/2}$)	R^2	K_{KP} (hour^{-n})	R^2	n
1:6	-	-	-	-	96.6	0.6964	0.01
1:2	5.75	0.67196	20.54	0.9748	16.8	0.9899	0.69
1:1	2.73	0.7111	9.50	0.9884	7.78	0.97178	0.67

Table S2 Parameters of the mathematical analysis of the curves of CytC release from the hydrogel formed by different Gua:GMP ratio (1:6, 1:2, and 1:1) at neutral pH, using the membraneless method for three models: Zero-order, Higuchi and Korsmeyer-Peppas

Formulations	**Zero-order**		**Higuchi**		**Korsmeyer–Peppas**		
	K_0(hour^{-1})	R^2	K_H (hour$^{-1/2}$)	R^2	K_{KP} (hour^{-n})	R^2	n
1:6	5.62	0.53245	33.3	0.8341	7.10	0.9537	1.28
1:2	2.62	0.93519	13.0	0.9678	1.59	0.8145	1.28
1:1	1.40	0.6602	7.86	0.8929	1.86	0.8054	1.04

Table S3 Parameters of the mathematical analysis of the curves of MB release from the hydrogel formed by 1:2 Gua:GMP ratio at different pH, using the membraneless method for three models: Zero-order, Higuchi and Korsmeyer-Peppas

pH	**Zero-order**		**Higuchi**		**Korsmeyer–Peppas**		
	K_0(hour^{-1})	R^2	K_H (hour$^{-1/2}$)	R^2	K_{KP} (hour^{-n})	R^2	n
3.0	7.88	0.86792	18.7	0.9439	26.7	0.9625	0.49
5.5	12.3	0.9010	30.3	0.9617	31.7	0.9475	0.59

7.4	12.3	0.8926	31.4	0.9805	36.8	0.9662	0.51
9.0	-	-	34.23	0.8053	80.4	0.5913	0.14